nature immunology

Article

https://doi.org/10.1038/s41590-025-02406-1

A GDF-15–GFRAL axis controls autoimmune T cell responses during neuroinflammation

Received: 9 March 2025

Accepted: 5 December 2025

Published online: 15 January 2026

Check for updates

Jana K. Sonner[1,2], Audrey Kahn[1,2], Lars Binkle-Ladisch[1,2], Jan Broder Engler[1,2], Beatrice Haack[3], Christina Zeiler[1,2], Lisa Unger[1,2], Simone Bauer[1,2], Felix Fischbach[1,2], Giovanni Almanzar[4], Mark Walkenhorst[1,2], Christina Mayer[1,2], Aneta Kolakowska[1,2], Sebastian Graute[5], Caren Ramien[1,2], Ingo Winschel[1,2], Nicola Rothammer[1,2], Markus Heine[5], Verena Horneffer-van der Sluis[6], Vincent Thiemann[3], Vanessa Vieira[1,2], Nina Meurs[1,2], Thomas Renné[6,7,8], Martina Prelog[4], Sebastian Beck Jørgensen[9], Randy J. Seeley[10], Anke Diemert[11], Petra C. Arck[2,11], Stefan M. Gold[1,12], Joerg Heeren[5], Jörg Wischhusen[3] & Manuel A. Friese[1,2]

Inflammatory activity during multiple sclerosis (MS) often improves during pregnancy, suggesting that pregnancy-related immune adaptations affect the disease. Here we show that growth/differentiation factor-15 (GDF-15) increases during pregnancy and correlates with a reduced rate of MS relapses. GDF-15 also accumulates in the inflamed central nervous system, and its absence impairs inflammation resolution in a mouse model of MS. GDF-15 suppresses autoimmune T cell responses through an indirect signaling pathway involving the activation of GDNF family receptor α-like (GFRAL) on brainstem neurons. Therapeutic approaches, including neuronal gene delivery, recombinant GDF-15 administration and targeted chemogenetic activation of GFRAL-positive neurons induce β-adrenergic signaling and norepinephrine synthesis in the spleen, leading to decreased expression of integrins on T cells required for transmigration across the blood–brain barrier and confer protection against neuroinflammation in preclinical models of MS. These findings position GDF-15 as a crucial neuroimmune mediator and the GDF-15–GFRAL axis as promising target for MS.

MS is a common neuroinflammatory disorder that primarily affects individuals in early adulthood. It likely arises from a dysregulated immune response directed against central nervous system (CNS) self-antigens, leading to inflammatory CNS lesions. Autoreactive T cells cross the blood–brain barrier, activate CNS-resident myeloid cells and drive progressive demyelination and neurodegeneration[1,2]. To counteract tissue inflammation, the body relies on inherent mechanisms of immune tolerance.

During pregnancy, a substantial reduction in inflammatory disease activity is observed in MS[3,4] and other T cell-mediated autoimmune diseases, such as rheumatoid arthritis or Graves' disease[5], emphasizing the potent immunomodulatory impact of pregnancy—effects partly reproduced in animal models[6–8]. Treatment with the pregnancy hormone estriol is effective in autoimmune encephalomyelitis[9] and shows some effects in clinical trials of nonpregnant women with MS, but does not fully recapitulate the pregnancy-related reduction in relapse rates[10]. This suggests that a more complex regulatory network governs transient tolerance during pregnancy. Elucidating the key mechanisms behind this evolutionarily selected immune tolerance, which allows the maternal body to accept the semi-allogeneic fetus, could be crucial for developing new therapeutic strategies for immune-mediated inflammatory diseases.

Bidirectional communication between the nervous and the immune system—immunoception—is receiving increasing attention,

A full list of affiliations appears at the end of the paper. e-mail: manuel.friese@zmnh.uni-hamburg.de

with evidence showing how immune imbalances activate specific brain regions and how neuronal regulation shapes inflammatory diseases[11–16]. One molecule that may link reduced inflammatory activity in pregnant individuals who have MS with neuronal control of peripheral immunity is GDF-15. During pregnancy, trophoblasts and immature dendritic cells in the placenta produce GDF-15, with maternal plasma concentrations rising as the fetus develops[17]. Most circulating GDF-15 originates from the fetus rather than maternal reproductive cells[18]. Low GDF-15 serum levels have been linked to miscarriage[19], suggesting a key role in fetal immune tolerance and potentially in suppressing autoreactive CNS-directed T cell responses. Consistently, GDF-15 suppresses lymphoproliferation in systemic lupus erythematosus[20].

Previous work identified GDNF family receptor α-like (GFRAL) as the canonical GDF-15 receptor responsible for inducing cachexia and anorexia[21,22]. GFRAL is primarily expressed in brainstem neurons[23], and no alternative immune cell receptor has been found, despite studies reporting direct T cell modulation by GDF-15[24], inhibition of neutrophil and macrophage chemotaxis[25,26], and reduced cytotoxicity of tumor-infiltrating macrophages[27], as well as GFRAL-independent modulation of myeloid cells[28]. GFRAL-expressing neurons cluster in the area postrema and to a lesser extent the nucleus tractus solitarius (NTS). Because these regions possess highly fenestrated capillaries, they are ideally positioned to sense soluble circulating mediators[29], including GDF-15 released by the fetus or from stressed tissues[18,30].

In this study, we explore how GDF-15 regulates autoimmune T cell responses downstream of GFRAL and demonstrate the effect of immunoception on neuroinflammation.

Results

GDF-15 expression is increased in human and mouse pregnancies

To assess whether GDF-15 contributes to fetomaternal immune tolerance, we measured its levels in human and mouse pregnancies. As reported[31], plasma GDF-15 gradually increased in human pregnancy compared to age-matched and body mass index-matched nonpregnant controls (Fig. 1a and Supplementary Table 1). In syngeneic C57BL/6J matings, we detected only a minor increase in systemic GDF-15 during the third trimester. In contrast, in semi-allogeneic matings, which mimic exposure to foreign antigens derived from the fetus, GDF-15 levels surged nearly fourfold (Extended Data Fig. 1a,b).

Although a study postulated that a lack of GDF-15 during human pregnancy has no impact on fetal development or pregnancy[32], we found that lower plasma GDF-15 in pregnant mice correlated with reduced litter size (Extended Data Fig. 1c). We further observed a striking difference between women experiencing a miscarriage and those undergoing an elective abortion (Fig. 1b and Supplementary Table 2). Notably, when stratifying pregnant individuals with MS according to their relapse activity during pregnancy, which can occasionally occur despite substantial pregnancy-related immunosuppression[3,4], we found that relapse activity was associated with reduced serum GDF-15 in early to mid-pregnancy (Fig. 1c and Supplementary Table 3). This finding suggests that pregnancy-induced GDF-15 may play a key role in mediating immunosuppression in the context of neuroinflammatory diseases.

CNS inflammation drives local GDF-15 expression

Because GDF-15 is induced by cellular stress[30], we investigated its regulation during CNS inflammation. In experimental autoimmune encephalomyelitis (EAE), *Gdf15* expression significantly increased during acute disease (15 days after EAE induction) in the spinal cord (Fig. 1d), the primary site of immune cell infiltration, microglia activation and neurodegeneration. Consistently, the increase in GDF-15 protein levels during acute EAE was more pronounced in the spinal cord than in the cortex (Extended Data Fig. 1d,e), whereas GDF-15 remained unchanged in the preclinical phase of the disease (Extended Data Fig. 1f). *Gdf15* transcript induction was most pronounced in nonneuronal cells, although neurons also significantly upregulated *Gdf15* expression during acute EAE (Fig. 1e and Supplementary Data Fig. 1a). This increase was similar in female and male mice (Extended Data Fig. 1g). Among nonneuronal cells, both astrocytes and microglia induced *Gdf15* expression during acute EAE (Fig. 1f and Supplementary Data Fig. 1b). However, the strongest *Gdf15* expression was detected in infiltrating myeloid cells (Fig. 1g and Extended Data Fig. 1h).

In accordance with previous reports using peripheral GDF-15 as a biomarker for neurodegenerative diseases[33,34], plasma GDF-15 levels were elevated in the chronic phase of the disease (29 days after EAE induction; Extended Data Fig. 1i,j), with no significant increase detected before disease onset (Extended Data Fig. 1k). Individuals with progressive MS also showed significantly elevated serum GDF-15 (Extended Data Fig. 1l and Supplementary Table 4). Although individuals with acute relapse events also exhibited increased GDF-15 levels, this effect was not statistically significant (Extended Data Fig. 1m and Supplementary Table 4). Together, these results suggest that GDF-15 is upregulated in response to acute inflammation within the spinal cord and can be detected in the circulation during chronic stages of neuroinflammatory diseases such as MS, where it may contribute to disease stability or regression[35].

To investigate which signals drive *Gdf15* expression, we generated a lentiviral GDF-15 reporter construct[36] that includes the putative *Gdf15* promoter sequence 1.7 kb upstream of the transcription start site, followed by a reporter fluorochrome (Supplementary Data Fig. 2a). We validated the *Gdf15*-mScarlet reporter in the neuronal cell line Neuro-2a using an inducer of the unfolded protein response, tunicamycin[37], resulting in a twofold increase in fluorescence intensity (Supplementary Data Fig. 2b). In primary neuron–astrocyte cultures, we observed a significant increase in *Gdf15* promoter activity in response to the NFE2-like bZIP transcription factor 2 (NRF2) activator 4-octyl itaconate (4-OI), which mimics downstream effects of oxidative stress, a hallmark of neuroinflammation[1], both in neurons and astrocytes (Supplementary Data Fig. 2c). Moreover, chronic stimulation with interferon-γ (IFNγ), a cytokine released by infiltrating T cells during autoimmune neuroinflammation[2], also increased *Gdf15* reporter expression in neurons and astrocytes (Fig. 1h,i). We corroborated this finding at the mRNA level (Fig. 1j). In microglia, *Gdf15* induction was limited to activation of Toll-like receptor 4 (TLR4) by lipopolysaccharide, but this effect was not statistically significant (Supplementary Data Fig. 2d,e). These findings suggest that upregulation of *Gdf15* in CNS-resident cells is orchestrated in a cell-type-specific manner in response to various molecular cues of cellular stress and inflammation.

Loss of *Gdf15* exacerbates CNS inflammation

Based on previous studies[35,38,39], we next hypothesized that GDF-15 induction during cellular stress initiates an immunoregulatory program that counteracts acute inflammation and protects neurons from inflammation-induced cell death. Although constitutive loss of *Gdf15* (ref. 40) did not alter EAE disease incidence or onset (Extended Data Fig. 2a,b), it significantly reduced survival (Fig. 1k) and worsened clinical outcomes during EAE (Fig. 1l–n and Extended Data Fig. 2c–e).

We found no significant difference in CNS immune cell infiltrates in *Gdf15*-deficient animals compared to control littermates during acute EAE (Extended Data Fig. 2f,g and Supplementary Data Fig. 3a). However, microglia in *Gdf15*-deficient animals exhibited increased expression of major histocompatibility complex class II and decreased expression of the purinergic receptor P2RY12 (Extended Data Fig. 2h and Supplementary Data Fig. 3b), indicating a pro-inflammatory phenotype. Additionally, we found increased expression of glycoprotein NMB (GPNMB), a phagocyte marker implicated in neurodegeneration[41], in infiltrating macrophages (Extended Data Fig. 2i and Supplementary Data Fig. 3b). Overall, these results suggest that GDF-15 mediates containment and resolution of neuroinflammation.

https://doi.org/10.1038/s41590-025-02406-1

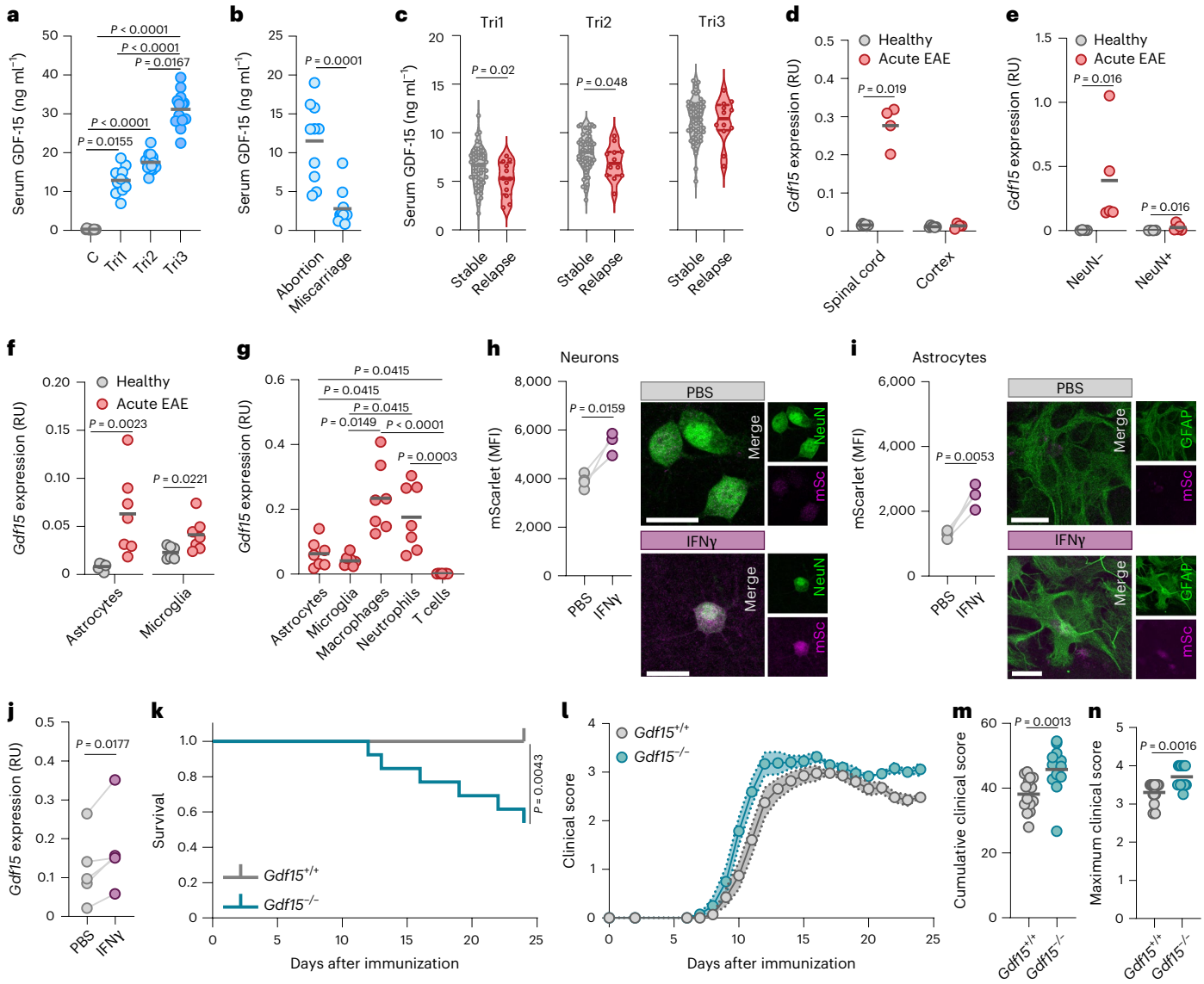

Fig. 1 | GDF-15 is induced in pregnancy and CNS inflammation. a, Serum levels of GDF-15 in pregnant women collected from trimester 1 (Tri1) to trimester 3 (Tri3), and age-matched and BMI-matched nonpregnant controls (C); $n = 13$. **b**, GDF-15 serum concentrations in women experiencing miscarriage and those undergoing elective abortion in Tri1; $n = 10$ per group. **c**, Serum concentrations of GDF-15 in individuals with MS throughout pregnancy stratified by stable disease ($n = 58$) versus relapse ($n = 12$) during pregnancy. **d**–**g**, *Gdf15* expression measured by quantitative PCR with reverse transcription (RT–qPCR) in **d**, spinal cord and cortex tissue of female healthy ($n = 6$) and acute EAE (day 15 post immunization (p.i.), $n = 4$) mice; **e**, spinal cord neuronal ($NeuN^+$) and nonneuronal ($NeuN^-$) nuclei of female healthy ($n = 4$) and acute EAE (day 15 p.i., $n = 5$) mice; **f**, spinal cord astrocytes and microglia of female healthy ($n = 6$) and acute EAE (day 15/16 p.i., $n = 7$) mice; and **g**, spinal cord astrocytes, microglia, macrophages, neutrophils and T cells in acute EAE (day 15/16 p.i.) mice; $n = 7$. **h**,**i**, Mean fluorescence intensity (MFI) of a P_{Gdf15}-mScarlet reporter in neurons (**h**) and astrocytes (**i**) after stimulation with 100 ng ml^{-1} IFNγ for 72 h; $n = 4$. Scale bars, 20 µm. **j**, *Gdf15* expression quantified by RT–qPCR in primary neuron–astrocyte co-cultures (14 days in vitro) treated with 100 ng ml^{-1} IFNγ for 72 h; $n = 5$. **k**–**n**, EAE was induced in $Gdf15^{+/+}$ ($n = 14$) and $Gdf15^{-/-}$ ($n = 13$) mice. **k**, Survival. **l**, Mean clinical score. **m**, Cumulative clinical score. **n**, Maximum clinical score. Individual data points represent biological replicates. Data are shown as the mean ± s.e.m. (**l**). In **a** and **g**, a Kruskal–Wallis test with false discovery rate (FDR) correction was performed. In **b**, **d**–**f**, **m** and **n**, two-sided Mann–Whitney tests were performed. In **c**, a Wilcoxon test was performed. In **h**–**j**, a two-sided paired *t*-test was performed. For **k**, a log-rank Mantel–Cox test was used. RU, relative units.

Therapeutic GDF-15 delivery protects against neuroinflammation

We next aimed to therapeutically harness GDF-15 to mitigate CNS inflammation. We developed a construct for direct mouse GDF-15 delivery to neurons using the human synapsin 1 promoter (Extended Data Fig. 3a). Transduction of primary neurons with a recombinant adeno-associated virus (rAAV) harboring this construct resulted in robust GDF-15 expression in neurons (Extended Data Fig. 3b) and secretion (Extended Data Fig. 3c). Using a low rAAV titer, intravenous injections for neuronal transduction achieved physiological plasma concentrations similar to those observed during late mouse pregnancy (Extended Data Fig. 3d) and high CNS expression (Extended Data Fig. 3e). As anticipated, due to GFRAL engagement and activation of anorexic effects[21,22], mice lost approximately 10% of body weight following neuronal GDF-15 delivery (Extended Data Fig. 3f).

In metabolic cages, these mice showed reduced food intake, energy expenditure and respiratory exchange ratio (Supplementary Data Fig. 4a–c), consistent with prior studies using recombinant GDF-15[42]. Notably, rAAV-mediated *Gdf15* delivery to the CNS completely prevented neuroinflammation (Fig. 2a–d and Supplementary

https://doi.org/10.1038/s41590-025-02406-1

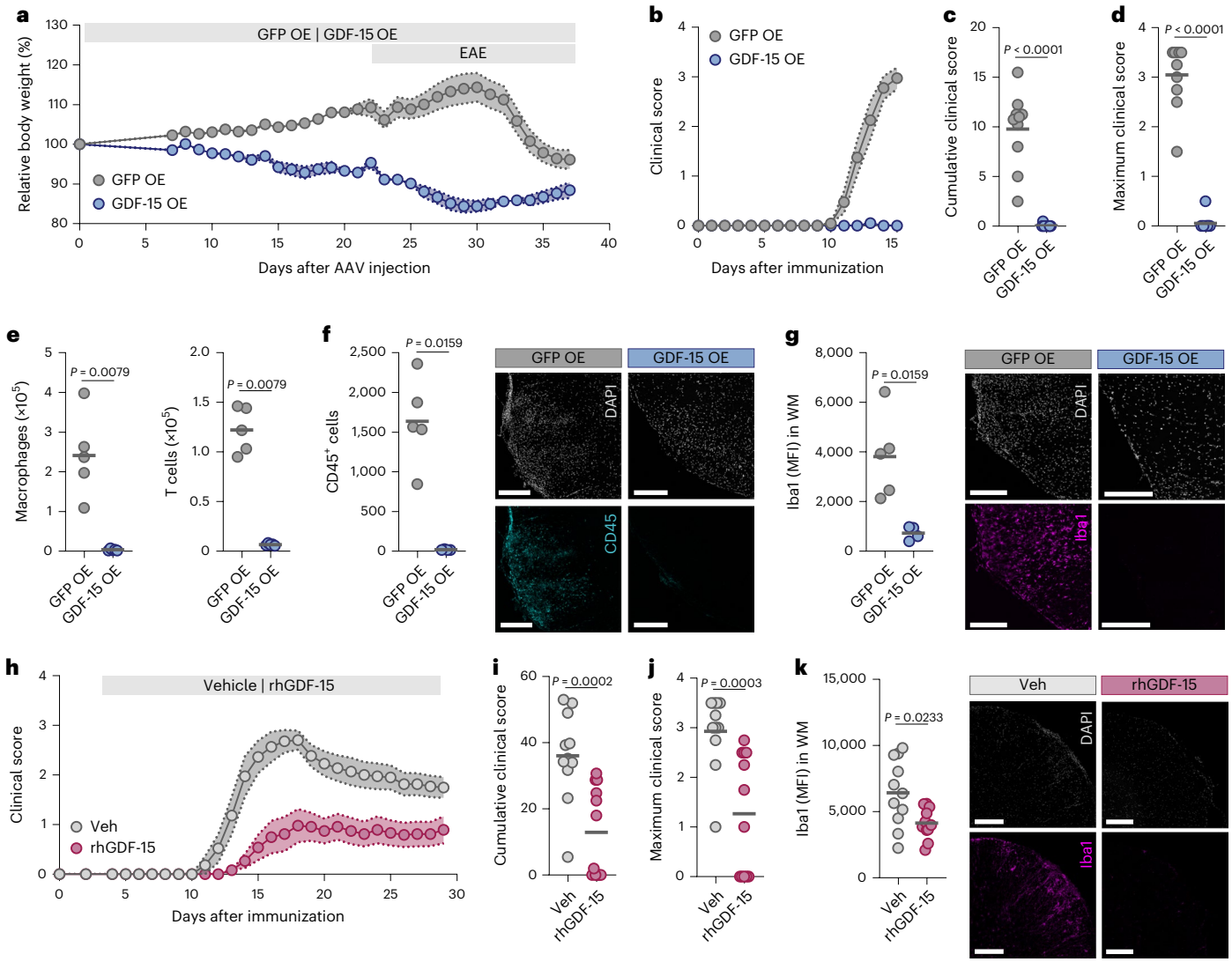

Fig. 2 | GDF-15 delivery is protective in neuroinflammation. a, Relative body weight change after injecting female C57BL/6J mice with an rAAV encoding eGFP (GFP OE, $n = 10$) or mouse GDF-15 (GDF-15 OE, $n = 9$). **b**, Mean clinical disease score. **c**, Cumulative disease score. **d**, Maximum disease score after immunization with $MOG_{35–55}$ 3 weeks after rAAV injection; $n = 10$ for GFP OE, $n = 9$ for GDF-15 OE. **e**, Absolute numbers of macrophages and T cells in brain and spinal cord tissue quantified by flow cytometry in acute EAE (day 15 p.i.); $n = 5$ per group. **f**, Quantification of infiltrating $CD45^+$ cells in cervical spinal cord sections in acute EAE (day 15 p.i.); $n = 5$ for GFP OE, $n = 4$ for GDF-15 OE. Scale bars, 200 µm. **g**, Mean fluorescence intensity (MFI) of Iba1 staining in the white matter (WM) of cervical spinal cord sections in acute EAE; $n = 5$ for GFP OE, $n = 4$ for GDF-15 OE. Scale bars, 200 µm. **h**–**k**, Female C57BL/6J mice were immunized with $MOG_{35–55}$ and received daily subcutaneous injections of 5 nmol per kg rhGDF-15 ($n = 12$) or a vehicle control (Veh, $n = 11$) from day 4 p.i. onward. **h**, Mean clinical score. **i**, Cumulative disease score. **j**, Maximum disease score. **k**, MFI of Iba1 staining in the WM of cervical spinal cord sections in chronic EAE (day 29 p.i.); $n = 11$ per group. Scale bars, 200 µm. Individual data points represent biological replicates. Data are shown as the mean ± s.e.m. (**a**, **b** and **h**). For **c**–**g** and **i**–**k**, Mann–Whitney tests were performed. OE, overexpression.

Data Fig. 5a) and we detected only a small number of CNS-infiltrating immune cells (Fig. 2e,f, Extended Data Fig. 3g and Supplementary Data Fig. 5b). This was accompanied by significantly reduced Iba1 and GFAP immunoreactivity, as well as lower numbers of $CD68^+$ myeloid cells in spinal cord sections from acute EAE animals (Fig. 2g, Extended Data Fig. 3h,i and Supplementary Data Fig. 5c,d). Together, inflammatory signals from both CNS-infiltrating and CNS-resident cells were diminished. Importantly, engagement of GFRAL by GDF-15 did not activate the hypothalamic–pituitary–adrenal axis[43], as plasma corticosterone remained unchanged (Extended Data Fig. 3j), suggesting that protection from neuroinflammation was not driven by corticosteroid-mediated immunosuppression.

Because GDF-15 reduces appetite via GFRAL[21,22] and we observed body weight loss after rAAV-mediated *Gdf15* delivery to the CNS (Fig. 2a and Extended Data Fig. 3f), we performed paired-feeding experiments to exclude caloric restriction as a confounder. While mice typically receive food ad libitum, an additional group with neuronal GFP overexpression (GFP OE) was pair-fed, receiving restricted amounts of food based on the intake of the GDF-15-overexpressing (GDF-15 OE) mice (Supplementary Fig. 6a). Despite caloric restriction, body weight loss in the pair-fed group was minimal (Supplementary Data Fig. 6b,c). In GDF-15 OE mice, weight loss was partly due to reduced fat mass, which was not observed in pair-fed GFP OE mice (Supplementary Data Fig. 6d). Importantly, pair-fed mice were not protected from neuroinflammation with similar disease severity and immune cell infiltration than GFP OE mice with ad libitum food access (Extended Data Fig. 3k–n and Supplementary Data Fig. 6e,f). Thus, caloric restriction alone does not account for GDF-15-mediated protection from neuroinflammation.

To evaluate clinical translatability, EAE mice received daily subcutaneous recombinant human GDF-15 (rhGDF-15; 5 nmol per kg of body

https://doi.org/10.1038/s41590-025-02406-1

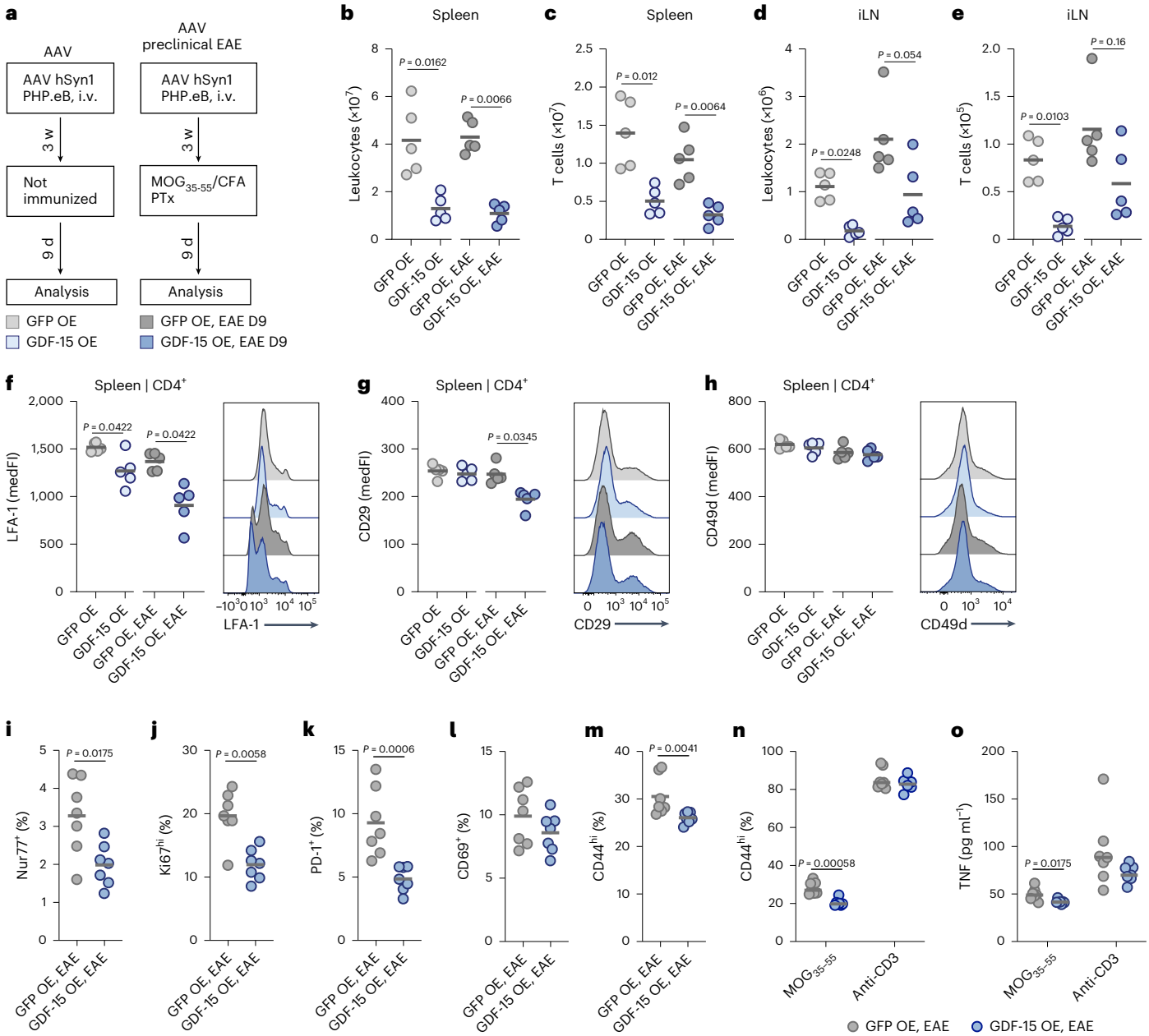

Fig. 3 | GDF-15 delivery suppresses peripheral CD4$^+$ T cell activation. Female C57BL/6J mice were injected with an rAAV encoding eGFP (GFP OE) or mouse GDF-15 (GDF-15 OE). In preclinical EAE groups, mice were immunized and organs were excised on day 9 p.i. before disease onset. **a**, Timeline for rAAV injection and EAE induction. i.v., intravenous. **b**–**e**, Absolute numbers quantified by flow cytometry; $n = 5$ per group. **b**, Leukocytes in the spleen. **c**, T cells in the spleen. **d**, Leukocytes in the inguinal lymph nodes (iLNs). **e**, T cells in the iLNs. **f**–**h**, Median fluorescence intensity (medFI) of selected markers on CD4$^+$ T cells in the spleen analyzed by flow cytometry; $n = 5$ per group. **f**, LFA-1. **g**, CD29. **h**, CD49d. **i**–**m**, Frequency of selected population within CD4$^+$ T cells in the spleen 9 days p.i. analyzed by flow cytometry; $n = 7$ per group. **i**, Nur77. **j**, Ki67. **k**, PD-1. **l**, CD69. **m**, CD44. **n**,**o**, Splenocytes were isolated 9 days p.i. and restimulated with 5 µg ml^{-1} MOG_{35-55} or 0.5 µg ml^{-1} anti-CD3 as a positive control; $n = 7$ per group. **n**, Frequency of CD44^{hi} cells within total CD4$^+$ T cells after 72 h. **o**, Concentration of tumor necrosis factor (TNF) in supernatant after 48 h. Individual data points represent biological replicates. For **b**–**o**, two-sided Mann–Whitney tests were used. OE, overexpression.

weight)[22,44]. Although this medium dose did not induce body weight loss (Extended Data Fig. 4a,b), it significantly reduced clinical disability and microglia activation, as indicated by decreased Iba1 reactivity in spinal cord white matter (Fig. 2h–k). We observed no differences in GFAP immunoreactivity, but fewer infiltrating leukocytes, T cells and CD68$^+$ myeloid cells (Extended Data Fig. 4c–e). In conclusion, both gene therapy and rhGDF-15 treatment were highly effective in preventing immune cell infiltration into the CNS, thereby protecting from neuroinflammation.

GDF-15 delivery suppresses CD4$^+$ T cell activation

We next sought to elucidate how GDF-15 impacts the recruitment of peripheral immune cells to the CNS. Following GDF-15 delivery to the CNS, we analyzed the peripheral immune cell compartments in preclinical EAE mice (9 days after immunization) and in healthy controls (Fig. 3a and Supplementary Data Fig. 7a). We detected a decrease in CD45$^+$ leukocytes, T cells and B cells in the spleen and inguinal lymph nodes (iLNs) in response to increased GDF-15 in both EAE mice and healthy controls (Fig. 3b–e and Supplementary Data Fig. 7b–d).

We next assessed integrins required for leukocyte rolling on endothelial cells[45] and T cell transmigration across the blood–brain barrier[2], specifically LFA-1 and VLA-4, the latter consisting of subunits CD29 and CD49d. We found that GDF-15 consistently downregulated the active, high-affinity conformation of LFA-1 on splenic (Fig. 3f) and iLN (Extended Data Fig. 5a) CD4$^+$ T cells, with weaker modulation of CD29 and CD49d (Fig. 3g,h and Extended Data Fig. 5b,c). The effect on LFA-1 expression was even more pronounced after EAE immunization. A similar pattern was observed for CD8$^+$ T cells (Supplementary Data Fig. 7e–g). Notably, downregulation of LFA-1 on CD4$^+$ and CD8$^+$ T cells was also evident in the CNS during acute EAE (Extended Data Fig. 5d).

To identify additional effector molecules beyond integrins, we isolated splenic CD4$^+$ T cells from the same experimental groups for bulk RNA sequencing (Extended Data Fig. 5e). We found that several checkpoint molecules increased expression following GDF-15 delivery, with *Il7r* identified as the top upregulated gene (Extended Data Fig. 5f–h). We validated increased protein expression of interleukin (IL)-7Rα—an exclusion marker for T cell activation[46]—and the inhibitory co-receptor B lymphocyte and T lymphocyte attenuator on splenic and iLN CD4$^+$ cells (Extended Data Fig. 5i,j).

Moreover, in splenic CD4$^+$ T cells during preclinical EAE (Supplementary Data Fig. 7h,i), GDF-15 delivery led to a pronounced downregulation of the immediate early activation marker Nur77 (Fig. 3i), the proliferation marker Ki67 (Fig. 3j) and additional indicators of T cell activation and memory formation, including programmed death-1 (PD-1), CD69 and CD44 (Fig. 3k–m). Restimulation of T cells from GDF-15 OE mice with $MOG_{35–55}$ peptide resulted in reduced memory T cell formation (Fig. 3n) and diminished secretion of tumor necrosis factor (Fig. 3o).

Together, elevation of GDF-15 not only reduces the overall T cell pool but also induces co-inhibitory molecules while suppressing LFA-1 expression, antigen-specific activation and proliferation, thereby limiting T cell transmigration into the CNS and pro-inflammatory functions.

GDF-15 delivery activates β-adrenergic signaling in the spleen

To explore how metabolic adaptation to GDF-15 delivery shapes autoimmune T cell responses, we performed plasma metabolomics. GDF-15 delivery to the CNS reduced systemic triglycerides, phosphatidylcholine and phosphatidylethanolamine species (Fig. 4a and Supplementary Table 5), with stronger effects following EAE induction (Extended Data Fig. 6a and Supplementary Table 6). This profile suggests increased lipolysis and decreased triglyceride synthesis, potentially resulting from sympathetic activation of adipose tissue[47,48].

Because GDF-15 has been linked to β-adrenergic signaling[44], we examined the expression of tyrosine hydroxylase (TH), the rate-limiting enzyme in catecholamine synthesis. Within the spleen, we detected TH$^+$ nerve fibers in close proximity to blood vessels (Fig. 4b) and GDF-15 delivery to the CNS nearly doubled TH expression in the spleen in naive and preclinical EAE mice (Fig. 4c), without affecting hepatic TH expression (Extended Data Fig. 6b). Based on a publication linking splenic sympathetic innervation to T cell exhaustion[49], we hypothesized that increased splenic TH expression after GDF-15 delivery might suppress autoimmune T cell responses through the release of norepinephrine or epinephrine. Consistent with this, we detected a local increase of splenic norepinephrine after GDF-15 delivery (Fig. 4d), while plasma norepinephrine remained unchanged (Extended Data Fig. 6c).

Indeed, treating primary mouse T cells with norepinephrine or epinephrine during T cell antigen receptor engagement significantly impaired proliferation and reduced the expression of the memory marker CD44 in CD4$^+$ T cells (Fig. 4e,f and Supplementary Data Fig. 8a). Moreover, CD69 expression and LFA-1 integrin levels were significantly decreased in CD4$^+$ T cells (Fig. 4g,h), whereas CD8$^+$ T cells were unaffected (Supplementary Data Fig. 8b,c). CD4$^+$ T cells expressed high levels of the β_2-adrenergic receptor (*Adrb2*), while the β_1-adrenergic receptor (*Adrb1*) was detected only at low levels (Extended Data Fig. 6d). Accordingly, selective activation of β_1-adrenergic or β_2-adrenergic receptors with the pharmacological agonists xamoterol or indacaterol revealed that β2-adrenergic receptor stimulation was more effective in suppressing CD4$^+$ T cell activation and LFA-1 expression (Extended Data Fig. 6e,f). Similarly, pretreatment of CD4$^+$ T cells with the β_2-adrenoreceptor antagonist ICI 118551 alleviated the suppressive effects of norepinephrine. In contrast, the β_1-adrenoreceptor antagonist CGP 20712A had little impact (Fig. 4i,j and Extended Data Fig. 6g). Genetic deletion of *Adrb2* in T cells completely abolished norepinephrine-induced downregulation of CD69 (Extended Data Fig. 6h).

Together, our findings suggest that GDF-15 engages the sympathetic nervous system to activate β_2-adrenergic signaling in splenic CD4$^+$ T cells, thereby suppressing autoimmune T cell responses.

GDF-15-mediated protection from neuroinflammation is GFRAL dependent

To determine whether GFRAL mediates immunosuppression in response to neuronal GDF-15 delivery, we generated a mutant version of mouse *Gdf15* that encodes an amino acid modification analogous to the p.Val87Arg mutation in human GDF-15, which is unable to bind to GFRAL[22]. Unlike native GDF-15, this mutated version abolished the weight loss associated with neuron-restricted expression (Extended Data Fig. 7a) and negated protection from neuroinflammation (Extended Data Fig. 7b–d). The immune cell infiltrate in the CNS of mice receiving GDF-15 p.Val90Arg resembled that of GFP controls (Extended Data Fig. 7e). We also administered the GDF-15 OE rAAV to *Gfral*-deficient mice[50], which showed no baseline deficits in body weight (Extended Data Fig. 8a). Consistent with our findings using the mouse GDF-15 p.Val90Arg, mice lacking *Gfral* expression did not lose body weight after neuronal GDF-15 delivery (Fig. 5a and Extended Data Fig. 8b). Furthermore, a significant reduction in spleen weight (Extended Data Fig. 8c), along with diminished total leukocytes and T cells in the spleen in response to GDF-15, was observed only in *Gfral*-proficient mice (Fig. 5b,c). This observation was replicated in the iLNs (Extended Data Fig. 8d,e), further corroborating that GDF-15-mediated modulation of the peripheral immune response is GFRAL dependent. We also validated that the downmodulation of LFA-1 on splenic CD4$^+$ T cells (Fig. 5d) and CD8$^+$ T cells (Extended Data Fig. 8f) is GFRAL dependent. Moreover, we demonstrated that GDF-15 delivery to the CNS reduces the frequency of effector memory CD4$^+$ T cells (Fig. 5e) and CD8$^+$ T cells (Extended Data Fig. 8g) only in *Gfral*-proficient mice.

In mouse pregnancies with physiologically elevated GDF-15 levels (Extended Data Fig. 1b) and additional complex physiological changes, we did not observe downregulation of CD44 or LFA-1, but rather a slight increase, which was mitigated in *Gfral*-deficient dams (Extended Data Fig. 8h,i). Consistent with our observations in healthy mice receiving neuronal GDF-15 delivery, we found that loss of GFRAL abolished the protective effects in EAE (Fig. 5f–i). While *Gfral*-proficient mice showed negligible immune cell infiltration in the CNS, *Gfral*-deficient mice displayed substantial immune cell infiltration (Fig. 5j and Extended Data Fig. 8j), underscoring GFRAL as the key sensor that coordinates the effector mechanisms exerted on peripheral immunity during neuroinflammation. In line with these results, sensing of increasing levels of endogenously released GDF-15 during neuroinflammation was also critical to limit chronic tissue inflammation. Although we did not observe any difference in disease incidence (Extended Data Fig. 9a), male *Gfral*-deficient mice showed a trend toward decreased survival (Extended Data Fig. 9b), potentially because they failed to recover from acute inflammation. In female mice, we did not observe any impact on survival, disease onset or maximum clinical score with *Gfral* loss (Extended Data Fig. 9b–d). However, the failure to sense endogenously produced GDF-15 via GFRAL led to greater disease severity during the chronic disease phase (Extended Data Fig. 9e–g).

https://doi.org/10.1038/s41590-025-02406-1

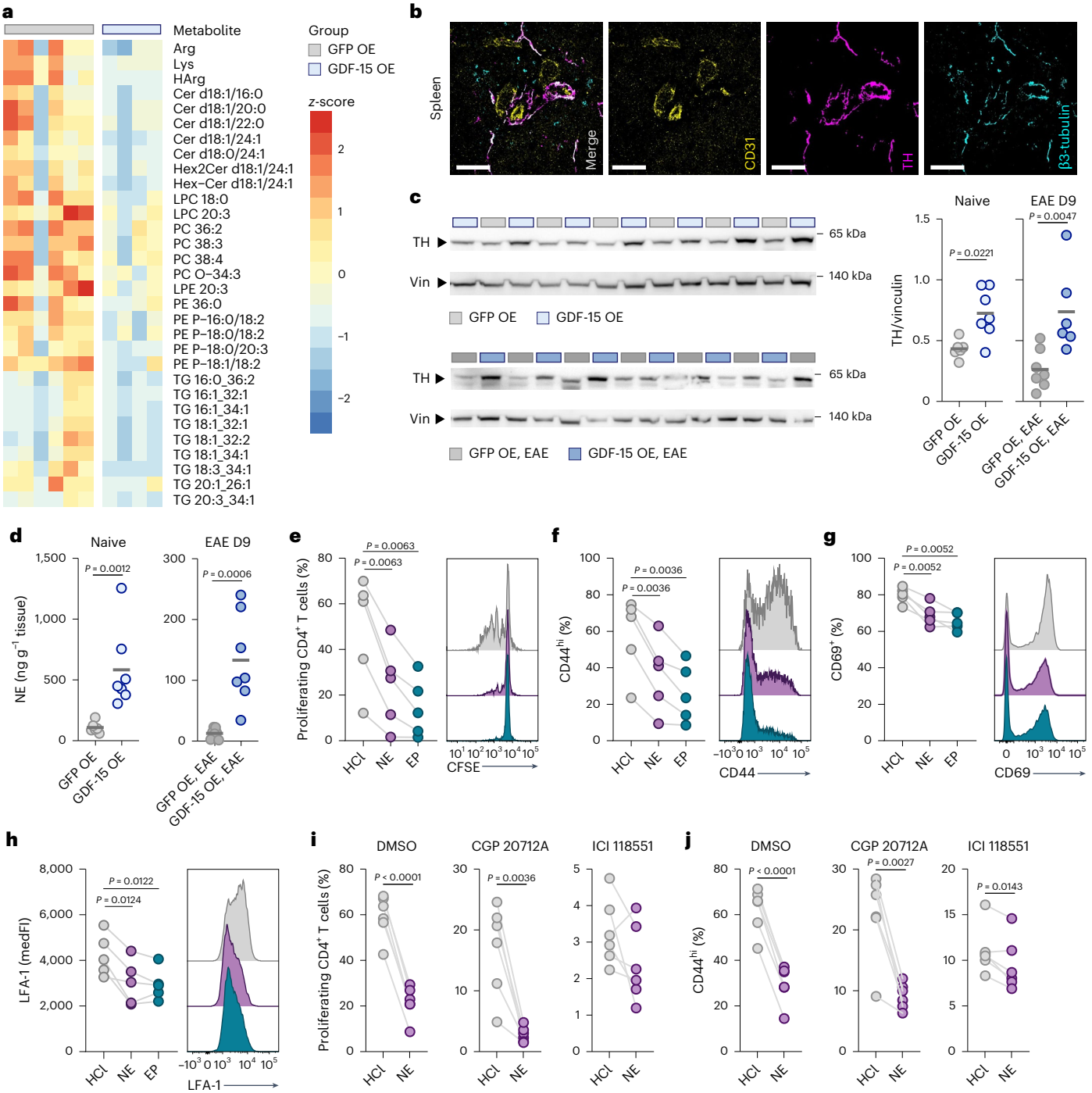

Fig. 4 | GDF-15 delivery activates β-adrenergic signaling in the spleen. **a**, Female C57BL/6J mice were injected with an rAAV encoding eGFP (GFP OE) or mouse GDF-15 (GDF-15 OE). Plasma was collected 3 weeks after rAAV injection for liquid chromatography–mass spectrometry analysis; $n = 6$ for GFP OE, $n = 4$ for GDF-15 OE. LPC, lysophosphatidylcholine; LPE, lysophosphatidylethanolamine; PC, phosphatidylcholine; PE, phosphatidylethanolamine; TG, triglyceride. **b**, Expression of tyrosine hydroxylase (TH) in spleen-innervating neurons surrounded by blood vessels. Scale bars, 100 µm. **c**,**d**, Female C57BL/6J mice were injected with an rAAV encoding GFP OE or GDF-15 OE. For EAE mice, organs were excised on day 9 p.i. **c**, Immunoblot for TH in the spleen of naive or preclinical EAE mice. Expression was normalized to vinculin (Vin). Naive: $n = 6$ for GFP OE, $n = 7$ for GDF-15 OE; EAE day 9: $n = 7$ for GFP OE, $n = 6$ for GDF-15 OE. **d**, Norepinephrine (NE) concentration in the spleens of naive or preclinical EAE mice normalized to tissue weight. Naive: $n = 6$ for GFP OE, $n = 7$ for GDF-15 OE; EAE day 9: $n = 7$ for GFP OE, $n = 7$ for GDF-15 OE. **e**–**h**, Primary mouse T cells were stimulated with anti-CD3/CD28 and 10 µM NE, 10 µM epinephrine (EP) or hydrochloric acid (HCl) as vehicle control; $n = 5$. **e**,**f**, Proliferation measured by CFSE dye dilution (**e**) and frequency of $CD44^{hi}$ cells (**f**) within total $CD4^+$ T cells after 72 h. **g**,**h**, Frequency of $CD69^+$ cells (**g**) and medFI of LFA-1 (**h**) in total $CD4^+$ T cells after 24 h. **i**,**j**, Primary mouse T cells were stimulated with anti-CD3/CD28 and 10 µM CGP 20712A, 10 µM ICI 118551 or dimethylsulfoxide (DMSO) as vehicle control before treatment with 10 µM NE or HCl; $n = 6$. **i**,**j**, Proliferation measured by CFSE dye dilution (**i**) and frequency of $CD44^{hi}$ cells (**j**) within total $CD4^+$ T cells after 72 h. Individual data points represent biological replicates. In **b**, data from one representative animal is shown. For **c** and **d**, two-sided Mann–Whitney tests were performed. For **e**–**h**, a paired one-way analysis of variance (ANOVA) with HCl as control group and FDR correction was performed. For **i** and **j**, paired two-sided *t*-tests were used. OE, overexpression.

Given that we identified β-adrenergic signaling as a potential mediator of GDF-15 on peripheral T cells, we measured TH expression in the spleens of *Gfral*-deficient mice and controls after GDF-15 delivery. Notably, the loss of GFRAL resulted in significantly reduced splenic TH expression in response to GDF-15 (Fig. 5k), and a decrease in splenic norepinephrine levels (Fig. 5l). Furthermore, genetic deletion of *Gfral* restored LFA-1 expression on CNS-infiltrating CD4$^+$ T cells after GDF-15 delivery (Fig. 5m).

To visualize GFRAL-expressing cells with high sensitivity, we next generated GFRAL reporter mice by crossing GFRAL-Cre mice[23] to Ai14 mice[51]. Consistent with earlier findings[23], we observed tdTomato$^+$ cells primarily in the area postrema and NTS region, with sparse labeling in other brain areas (Fig. 5n and Extended Data Fig. 10a). We also identified tdTomato labeling in the spinal cord (Extended Data Fig. 10b). Of note, tdTomato colocalized with the neuronal marker NeuN$^+$, but not with astrocyte, microglia or endothelial cell markers (Extended Data Fig. 10c,d). We quantified tdTomato expression in the CNS and spleen using immunoblotting, confirming the absence of GFRAL expression in peripheral lymphoid organs (Extended Data Fig. 10e). Additionally, we validated the lack of *Gfral* expression in the spleen by quantifying mRNA expression (Extended Data Fig. 10f,g).

To exclude direct effects of GDF-15 on immune cells, we utilized phosphorylated Erk1/Erk2 (pErk1/pErk2) as a downstream signaling marker of GFRAL[21,22]. Both *Gfral*-proficient and *Gfral*-deficient leukocytes stimulated with recombinant GDF-15 showed no increase in pErk1/pErk2 levels (Fig. 5o), whereas this response was observed in Neuro-2a cells expressing both GFRAL and the co-receptor Ret (Extended Data Fig. 10h). In summary, our results indicate that GFRAL expression in the CNS is essential for GDF-15-induced protection from neuroinflammation via engagement of splenic β-adrenergic signaling.

Selective activation of GFRAL$^+$ neurons prevents neuroinflammation

Lastly, to test whether activation of GFRAL$^+$ neurons is sufficient to replicate the effects of GDF-15 delivery, we used designer receptors exclusively activated by designer drugs (DREADD) technology[52]. We crossed GFRAL-Cre mice[23] to LSL-hM3Dq-DREADD mice[53], leading to expression of the mutant activating G-protein-coupled receptor hM3Dq specifically in GFRAL$^+$ cells. We confirmed expression in area postrema and NTS neurons using an antibody directed against the hemagglutinin (HA)-tag, alongside visualization of the coexpressed mCitrine fluorochrome (Fig. 6a and Supplementary Data Fig. 9a,b). After administration of clozapine-*N*-oxide (CNO), which activates hM3Dq, only Cre$^+$ mice showed 5–10% body weight loss (Fig. 6b,c). Chemogenetic activation of GFRAL$^+$ neurons was sufficient to prevent clinical symptoms of neuroinflammation (Fig. 6d–f) and abolished immune cell infiltration into the spinal cord (Fig. 6g). Selective activation of GFRAL$^+$ neurons also increased TH expression and norepinephrine accumulation in the spleen in the preclinical EAE phase (Fig. 6h,i). Additionally, LFA-1 expression was reduced in splenic CD4$^+$ T cells (Fig. 6j) and CNS-invading CD4$^+$ T cells (Fig. 6k). Thus, our data demonstrate that selective activation of GFRAL$^+$ neurons induces β-adrenergic signaling in the spleen and effectively blocks neuroinflammation by preventing the infiltration of autoimmune T cells.

Discussion

In this study, we investigated the role of GDF-15 in limiting neuroinflammation. Consistent with previous studies[17], we identified that GDF-15 accumulates in human and mouse pregnancies as a consequence of changes in the fetal and maternal secretome. The observation that individuals with MS protected from relapses during pregnancy showed higher serum levels of GDF-15 prompted us to hypothesize that GDF-15 suppresses autoreactive T cells by engaging GFRAL on brainstem neurons. We identified GDF-15 as essential for restraining chronic CNS inflammation. Mice lacking GDF-15 experienced more severe EAE, failed to recover and exhibited a pro-inflammatory microglia and infiltrating myeloid cell phenotype. This finding is consistent with its tissue-protective properties during inflammation-induced cardiac failure[38] and muscle injury[39].

We further discovered that CNS-resident and infiltrating immune cells upregulate *Gdf15* expression during acute CNS inflammation. In addition to established molecular cues, such as the unfolded protein response[37] and oxidative stress[54], both hallmarks of MS[1], T cell-derived cytokines such as IFNγ also induce *Gdf15* in neurons and glial cells. While previous studies suggested that IFNγ signaling raises systemic GDF-15 levels in infection models indirectly[55], our data indicate that IFNγ directly induces GDF-15 in neuroinflammation[2].

Using gene therapy, we demonstrated that delivering GDF-15 to the CNS is sufficient to block immune cell infiltration and protect animals from EAE. Notably, this approach achieved plasma levels of GDF-15, comparable to those observed during late mouse pregnancy, when the suppression of autoimmune neuroinflammation is most pronounced[3,4]. Importantly, the protection from neuroinflammation could not be reproduced by caloric restriction, as pair-fed mice remained fully susceptible to EAE induction. In a complementary approach, administering recombinant native human GDF-15—originally developed to improve insulin sensitivity and treat obesity[21,22,44]—after EAE induction drastically alleviated neuroinflammation. Although clinical trials exploring GDF-15 for obesity treatment have been discouraging due to an insufficient reduction in body weight[56,57], these studies have demonstrated the safety of administering GDF-15 analogs to humans. Our study suggests that the suppression of neuroinflammation by rhGDF-15 is uncoupled from body weight loss. Given the accessibility of brainstem GFRAL$^+$ neurons via fenestrated capillaries[29], clinically tested GDF-15 agonists may be repurposed to treat autoimmune diseases such as MS.

A previous report indicated that tumor-derived GDF-15 can impair T cell recruitment by limiting integrin-mediated adhesion to the vasculature, a process that can be reversed using a neutralizing GDF-15

Fig. 5 | GDF-15-mediated protection from neuroinflammation is GFRAL dependent. a–**e**, Female mice were injected with an rAAV encoding eGFP (GFP OE) or mouse GDF-15 (GDF-15 OE); $n = 5$ for *Gfral*$^{+/+}$ GFP OE, $n = 5$ for *Gfral*$^{+/+}$ GDF-15 OE, $n = 7$ for *Gfral*$^{-/-}$ GFP OE, $n = 6$ for *Gfral*$^{-/-}$ GDF-15 OE. **a**, Relative body weight change 3 weeks after rAAV injection. **b**,**c**, Absolute number of splenic CD45$^+$ leukocytes (**b**) and T cells (**c**). **d**, MedFI of LFA-1 on splenic CD4$^+$ T cells. **e**, Frequency of CD44^{hi} CD4$^+$ T cells in the spleen. **f**–**j**, Female *Gfral*-proficient and *Gfral*-deficient mice were injected with a GDF-15 OE rAAV and EAE was induced 3 weeks later; $n = 4$ for *Gfral*$^{+/+}$, $n = 5$ for *Gfral*$^{-/-}$. **f**, Relative body weight changes. **g**, Mean clinical score. **h**, Cumulative clinical score. **i**, Maximum clinical score. **j**, Absolute number of immune cells in spinal cord and brain tissue quantified by flow cytometry on day 15 p.i. **k**, Immunoblot for TH in the spleen of female GDF-15 OE mice on day 9 p.i. Expression was normalized to vinculin (Vin); $n = 6$ for *Gfral*$^{+/+}$, $n = 7$ for *Gfral*$^{-/-}$. **l**, Norepinephrine (NE) concentration in the spleens of male and female GDF-15 OE mice normalized to tissue weight; $n = 6$ for *Gfral*$^{+/+}$, $n = 7$ for *Gfral*$^{-/-}$. **m**, MedFI of LFA-1 on CD4$^+$ T cells in the CNS during acute EAE (day 15 p.i.); $n = 4$ for *Gfral*$^{+/+}$, $n = 5$ for *Gfral*$^{-/-}$. **n**, Expression of tdTomato in the area postrema and NTS in GFRAL-Cre × Ai14 mice. Scale bars, 200 µm. **o**, Splenocytes from *Gfral*$^{+/+}$ and *Gfral*$^{-/-}$ mice were stimulated with increasing doses of recombinant human GDF-15 (rhGDF-15), 100 ng ml^{-1} phorbol 12-myristate 13-acetate (PMA) or sodium acetate (NaAc) as a vehicle control for 30 min. MedFI of pErk1/pErk2 was determined in total leukocytes (CD45$^+$); $n = 3$ per group. Individual data points represent biological replicates. Data are shown as the mean ± s.e.m. (**f** and **g**). In **n**, data from one representative animal are shown. In **a**–**e**, two-way ANOVA with FDR correction was performed. For **g**–**m**, two-sided Mann–Whitney tests were performed. Data in **o** were analyzed with a paired one-way ANOVA with FDR correction. OE, overexpression.

https://doi.org/10.1038/s41590-025-02406-1

antibody[24]. This approach has recently been successfully translated into clinical application for solid tumors[58]. However, the authors showed that this direct effect on immune cells is independent of GFRAL[24], which up to now is the only known receptor for GDF-15[21,22]. Thus, we cannot exclude the possibility of GFRAL-independent immunomodulatory effects, as supported by a study showing that GDF-15 mediates anti-inflammatory effects in the liver in the presence of neutralizing anti-GFRAL antibodies, RET inhibitors or in *Gfral*-deficient mice[28].

To resolve the discrepancy between GFRAL-dependent and GFRAL-independent effects, we combined a mutant GDF-15 lacking GFRAL-binding activity with studies in *Gfral*-deficient mice[50], demonstrating that GDF-15-mediated protection from neuroinflammation is GFRAL dependent. Also, GDF-15, produced physiologically in response to neuroinflammation, acted as an endogenous brake to limit chronic tissue inflammation via activation of GFRAL$^+$ neurons, since EAE was exacerbated in the late disease phase in *Gfral*-deficient mice. While the lack of GFRAL expression on immune cells has been postulated for many years, this conclusion mainly relied on mRNA expression analysis[24]. In contrast, our use of GFRAL reporter mice and functional assays on leukocytes now excludes direct GDF-15–GFRAL

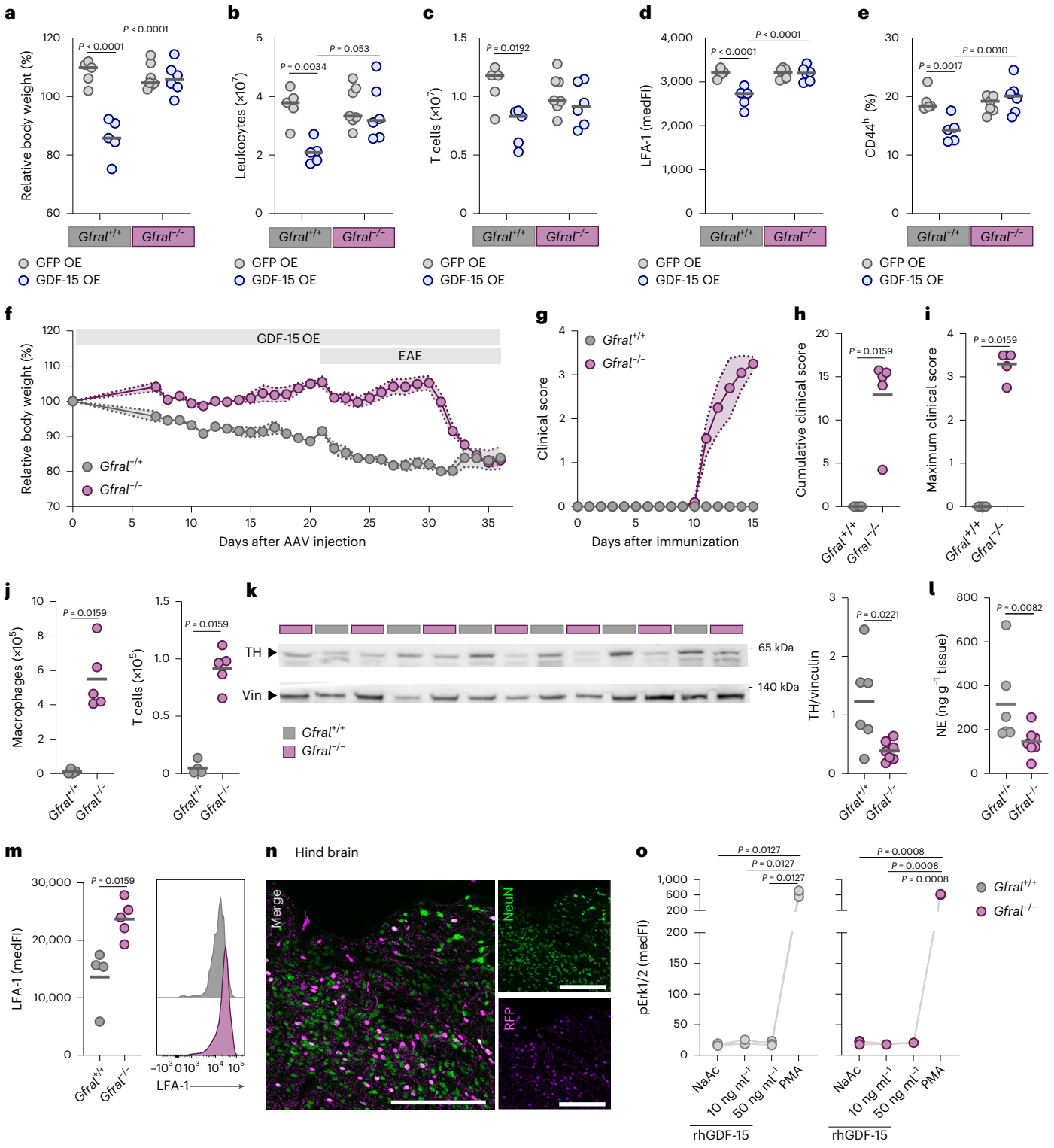

https://doi.org/10.1038/s41590-025-02406-1

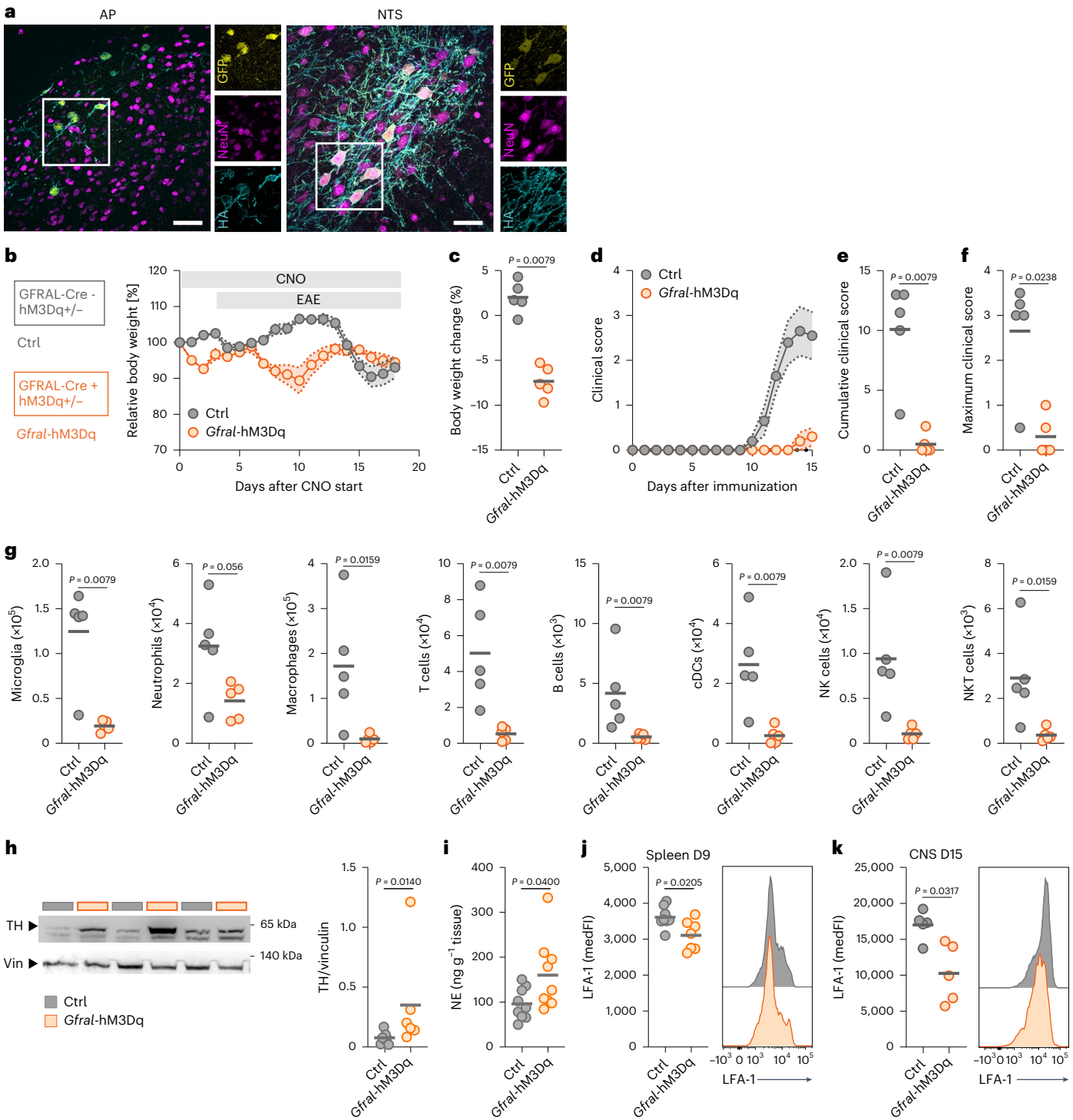

Fig. 6 | Chemogenetic activation of GFRAL$^+$ neurons prevents neuroinflammation. a, Expression of hM3Dq in neurons of the area postrema (AP) and NTS in GFRAL-Cre × LSL-hM3Dq-DREADD (*Gfral*-hM3Dq) animals. Scale bars, 50 µm. **b**–**k**, Female and male mice expressing an activating DREADD in GFRAL$^+$ cells (*Gfral*-hM3Dq) and Cre-negative littermates (Ctrl) received 4 µg ml^{-1} clozapine-*N*-oxide (CNO) in drinking water. Three days later, mice were immunized for EAE induction. **b**, Relative body weight. **c**, Body weight change after 48 h of CNO administration. **d**, Clinical score. **e**, Cumulative disease score. **f**, Maximum clinical score; $n = 5$ per group. **g**, Absolute number of microglia, macrophages, neutrophils, T cells, B cells, conventional dendritic cells (cDCs), natural killer (NK) cells and NK T cells in spinal cord quantified by flow cytometry on day 15 p.i.; $n = 5$ per group. **h**, Representative immunoblot for TH in the spleen on day 9 p.i. Expression was normalized to vinculin (Vin); $n = 7$ for Ctrl, $n = 6$ for *Gfral*-hM3Dq. **i**, Norepinephrine (NE) concentration in the spleen on day 9 p.i. normalized to tissue weight; $n = 9$ for Ctrl, $n = 9$ for *Gfral*-hM3Dq. **j**, MedFI of LFA-1 on CD4$^+$ T cells in the spleen on day 9 p.i.; $n = 8$ for Ctrl, $n = 7$ for *Gfral*-hM3Dq. **k**, MedFI of LFA-1 on CD4$^+$ T cells in the CNS during acute EAE (day 15 p.i.); $n = 5$ per group. Individual data points represent biological replicates. Data are shown as the mean ± s.e.m. (**b** and **d**). In **a**, data from one representative animal is shown. For **c**–**k**, two-sided Mann–Whitney tests were performed.

https://doi.org/10.1038/s41590-025-02406-1

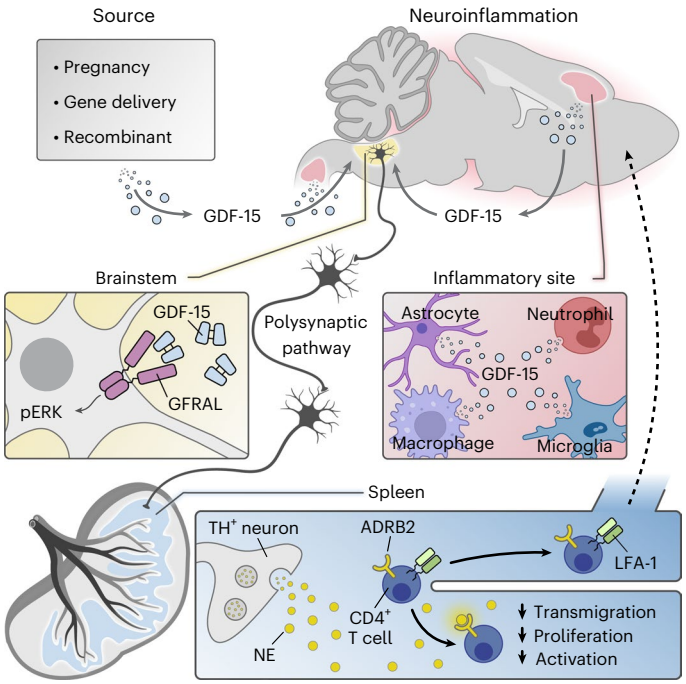

Fig. 7 | Working model of immunoception in neuroinflammation. High levels of GDF-15, released in response to pregnancy or in response to therapeutic delivery, or secreted from the inflamed tissue during neuroinflammation, are sensed by GFRAL-expressing neurons in the brainstem. Activation of a polysynaptic pathway downstream of GFRAL$^+$ neurons stimulates β-adrenergic signaling in the spleen. As a consequence, TH$^+$ neurons release NE and activate β_2-adrenergic receptors (ADRB2) on CD4$^+$ T cells, which dampens surface expression of the integrin LFA-1 and reduces activation and proliferation. This modulation of autoreactive T cells prevents transmigration to the CNS, thereby limiting neuroinflammation.

engagement on immune cells. Instead, using DREADD technology[52,53] to specifically activate GFRAL$^+$ neurons, we showed that neuronal activation is sufficient to confer protection against neuroinflammation. This indicates that the purview of this small subpopulation of GFRAL$^+$ brainstem neurons goes beyond metabolic adaptation in the context of thermoregulation, weight loss or energy expenditure[21,22,42,59]. Notably, our therapeutic approach was independent of corticosterone-induced immunosuppression via the hypothalamic–pituitary–adrenal axis[43] and instead modulates immunity through the sympathetic nervous system, which activates β-adrenergic signaling in the spleen—a major reservoir of T cells that can access the CNS during neuroinflammation[60].

Although earlier studies noted that GDF-15 stimulates triglyceride export in response to bacterial and viral infections[61], it was not addressed whether central GFRAL$^+$ neurons activation is required. While the projection landscape of GFRAL$^+$ neurons has been mapped only within the CNS[23], it is possible that they also project to peripheral anatomical regions such as the celiac plexus to regulate splenic immune responses, as previously shown for other brainstem neurons[62]. Further investigations are needed to decipher whether this regulation of peripheral immunity is mediated by CNS-intrinsic projections to different brain regions, or by projections to the peripheral nervous system that innervate lymphoid organs.

Mechanistically, we found that GDF-15 engagement of GFRAL downregulates the high-affinity conformation of the integrin LFA-1 and reduces T cell numbers in secondary lymphoid organs before the onset of EAE symptoms. This modulation is reversed by *Gfral* deletion and mimicked by chemogenetic activation of GFRAL$^+$ neurons.

Although previous reports suggested that GDF-15 can directly modulate integrin activation on immune cells[24,38], our findings indicate that central engagement of GFRAL in circumventricular organs by GDF-15 has a stronger influence on peripheral immunity. Furthermore, we showed that therapeutic GDF-15 delivery impairs peripheral T cell activation and proliferation. Based on these observations, we postulate that GDF-15-mediated impairment of T cell proliferation, activation and integrin expression in secondary lymphoid organs acts synergistically to protect from neuroinflammation. Inspired by previous studies on splenic sympathetic innervation affecting T cell exhaustion in cancer[49], we demonstrated that activation of β-adrenergic signaling in the spleen can explain the modulation of autoimmune T cell responses. Ex vivo stimulation of T cells with norepinephrine and epinephrine, but also selective β_2-adrenergic receptor agonists, decreased LFA-1 expression and activation of CD4$^+$ T cells, whereas pharmacological inhibition or genetic deletion of ADRB2 abolished these effects.

Based on our observations, we propose the following model (see graphical summary in Fig. 7): high levels of GDF-15, whether produced during pregnancy or in response to therapeutic delivery, or released within the inflamed neural tissue, enter the bloodstream and access central GFRAL$^+$ neurons via fenestrated capillaries. Activation of these neurons triggers a polysynaptic cascade that leads to norepinephrine release from TH$^+$ neurons into the spleen and possibly other secondary lymphoid organs. Engagement of β_2-adrenoreceptors on CD4$^+$ T cells results in downregulation of high-affinity LFA-1, and reduced T cell activation, proliferation and trafficking, ultimately protecting against neuroinflammation. This precise modulation of peripheral immunity by a small population of brainstem neurons exemplifies a fine-tuned evolutionary adaptation that controls aberrant autoimmune responses. It can, therefore, be considered a prime example of immunoception[11], a term that was coined to describe the brain's bidirectional monitoring and control of immunity. As such, our findings enhance our understanding of neuroimmune interactions and have broad implications for inflammatory diseases including MS.

A limitation of this study is that we could not detect the T cell-modulatory effects of therapeutic GDF-15 delivery in the context of mouse pregnancies. Although rAAV-mediated CNS expression effectively recalibrated T cell responses, high endogenous GDF-15 levels during pregnancy did not reduce LFA-1 expression or memory formation in CD4$^+$ T cells. Consistently, genetic loss of *Gfral* in pregnant mice did not alter T cell responses, in contrast to the effects observed during CNS inflammation.

This context-specific difference may reflect a protective physiological adaptation. During pregnancy, excessive GDF-15 signaling can induce appetite loss and nausea, and rare genetic hyperactivation is linked to hyperemesis gravidarum[18]. To safeguard maternal nutrition, pregnancy may therefore attenuate GDF-15–GFRAL signaling. Supporting this possibility, membrane-bound matrix metalloproteinase 14 has been shown to mediate proteolytic cleavage of GFRAL and thereby reduce GDF-15 responsiveness in obesity[63]. A similar mechanism during pregnancy could limit peripheral immune recalibration despite elevated circulating GDF-15.

Future studies should explore how GFRAL expression and shedding are regulated during pregnancy and whether complementary immune checkpoints compensate to protect fetal development when GDF-15–GFRAL signaling is constrained. Additionally, the potential existence of an additional GDF-15 receptor remains unresolved, and its identification may help explain pregnancy complications associated with low GDF-15 levels[19] despite the putative lack of GFRAL surface expression.

Online content

Any methods, additional references, Nature Portfolio reporting summaries, source data, extended data, supplementary information, acknowledgements, peer review information; details of author contributions and competing interests; and statements of data and code availability are available at https://doi.org/10.1038/s41590-025-02406-1.

References

1. Woo, M. S., Engler, J. B. & Friese, M. A. The neuropathobiology of multiple sclerosis. *Nat. Rev. Neurosci.* **25**, 493–513 (2024).
2. Attfield, K. E., Jensen, L. T., Kaufmann, M., Friese, M. A. & Fugger, L. The immunology of multiple sclerosis. *Nat. Rev. Immunol.* **22**, 734–750 (2022).
3. Schubert, C. et al. Postpartum relapse risk in multiple sclerosis: a systematic review and meta-analysis. *J. Neurol. Neurosurg. Psychiatry* **94**, 718–725 (2023).
4. Gold, S. M. & Voskuhl, R. R. Pregnancy and multiple sclerosis: from molecular mechanisms to clinical application. *Semin. Immunopathol.* **38**, 709–718 (2016).
5. Piccinni, M. P. et al. How pregnancy can affect autoimmune diseases progression?. *Clin. Mol. Allergy* **14**, 11 (2016).
6. Munoz-Suano, A., Kallikourdis, M., Sarris, M. & Betz, A. G. Regulatory T cells protect from autoimmune arthritis during pregnancy. *J. Autoimmun.* **38–178**, J103–J108 (2012).
7. Landek-Salgado, M. A., Rose, N. R. & Caturegli, P. Placenta suppresses experimental autoimmune hypophysitis through soluble TNF receptor 1. *J. Autoimmun.* **38**, J88–J96 (2012).
8. Engler, J. B. et al. Glucocorticoid receptor in T cells mediates protection from autoimmunity in pregnancy. *Proc. Natl Acad. Sci. USA* **114**, E181–E190 (2017).
9. Spence, R. D. & Voskuhl, R. R. Neuroprotective effects of estrogens and androgens in CNS inflammation and neurodegeneration. *Front. Neuroendocrinol.* **33**, 105–115 (2012).
10. Voskuhl, R. R. et al. Estriol combined with glatiramer acetate for women with relapsing-remitting multiple sclerosis: a randomised, placebo-controlled, phase 2 trial. *Lancet Neurol.* **15**, 35–46 (2016).
11. Koren, T. & Rolls, A. Immunoception: defining brain-regulated immunity. *Neuron* **110**, 3425–3428 (2022).
12. Koren, T. et al. Insular cortex neurons encode and retrieve specific immune responses. *Cell* **184**, 5902–5915 (2021).
13. Schiller, M. et al. Optogenetic activation of local colonic sympathetic innervations attenuates colitis by limiting immune cell extravasation. *Immunity* **54**, 1022–1036 (2021).
14. Klein Wolterink, R. G. J., Wu, G. S., Chiu, I. M. & Veiga-Fernandes, H. Neuroimmune interactions in peripheral organs. *Annu. Rev. Neurosci.* **45**, 339–360 (2022).
15. Jin, H., Li, M., Jeong, E., Castro-Martinez, F. & Zuker, C. S. A body–brain circuit that regulates body inflammatory responses. *Nature* **630**, 695–703 (2024).
16. Wheeler, M. A. & Quintana, F. J. The neuroimmune connectome in health and disease. *Nature* **638**, 333–342 (2025).
17. Wischhusen, J., Melero, I. & Fridman, W. H. Growth/differentiation factor-15 (GDF-15): from biomarker to novel targetable immune checkpoint. *Front. Immunol.* **11**, 951 (2020).
18. Fejzo, M. et al. GDF15 linked to maternal risk of nausea and vomiting during pregnancy. *Nature* **625**, 760–767 (2023).
19. Tong, S. et al. Serum concentrations of macrophage inhibitory cytokine 1 (MIC 1) as a predictor of miscarriage. *Lancet* **363**, 129–130 (2004).
20. Lorenz, G. et al. GDF15 suppresses lymphoproliferation and humoral autoimmunity in a murine model of systemic lupus erythematosus. *J. Innate Immun.* **14**, 673–689 (2022).
21. Mullican, S. E. et al. GFRAL is the receptor for GDF15 and the ligand promotes weight loss in mice and nonhuman primates. *Nat. Med.* **23**, 1150–1157 (2017).
22. Yang, L. et al. GFRAL is the receptor for GDF15 and is required for the anti-obesity effects of the ligand. *Nat. Med.* **23**, 1158–1166 (2017).
23. Sabatini, P. V. et al. GFRAL-expressing neurons suppress food intake via aversive pathways. *Proc. Natl Acad. Sci. USA* **118**, e2021357118 (2021).
24. Haake, M. et al. Tumor-derived GDF-15 blocks LFA-1 dependent T cell recruitment and suppresses responses to anti-PD-1 treatment. *Nat. Commun.* **14**, 4253 (2023).
25. Santos, I. et al. CXCL5-mediated recruitment of neutrophils into the peritoneal cavity of Gdf15-deficient mice protects against abdominal sepsis. *Proc. Natl. Acad. Sci. USA* **117**, 12281–12287 (2020).
26. de Jager, S. C. A. et al. Growth differentiation factor 15 deficiency protects against atherosclerosis by attenuating CCR2-mediated macrophage chemotaxis. *J. Exp. Med.* **208**, 217–225 (2011).
27. Ratnam, N. M. et al. NF-κB regulates GDF-15 to suppress macrophage surveillance during early tumor development. *J. Clin. Invest.* **127**, 3796–3809 (2017).
28. Weng, J. -H. et al. Colchicine acts selectively in the liver to induce hepatokines that inhibit myeloid cell activation. *Nat. Metab.* **3**, 513–522 (2021).
29. Cheng, W. et al. Hindbrain circuits in the control of eating behaviour and energy balance. *Nat. Metab.* **4**, 826–835 (2022).
30. Wang, D. et al. GDF15: emerging biology and therapeutic applications for obesity and cardiometabolic disease. *Nat. Rev. Endocrinol.* **17**, 592–607 (2021).
31. Moore, A. G. et al. The transforming growth factor-ss superfamily cytokine macrophage inhibitory cytokine-1 is present in high concentrations in the serum of pregnant women. *J. Clin. Endocrinol. Metab.* **85**, 4781–4788 (2000).
32. Gurtan, A. M. et al. Identification and characterization of human GDF15 knockouts. *Nat. Metab.* **6**, 1913–1921 (2024).
33. Walker, K. A. et al. Proteomics analysis of plasma from middle-aged adults identifies protein markers of dementia risk in later life. *Sci. Transl. Med.* **15**, eadf5681 (2023).
34. Guo, Y. et al. Plasma proteomic profiles predict future dementia in healthy adults. *Nat. Aging* **4**, 247–260 (2024).
35. Amstad, A. et al. Growth differentiation factor 15 is increased in stable MS. *Neurol. Neuroimmunol. Neuroinflamm.* **7**, e675 (2020).
36. Lu, J. F. et al. GDF15 is a major determinant of ketogenic diet-induced weight loss. *Cell Metab.* **35**, 2165–2182 (2023).
37. Patel, S. et al. GDF15 provides an endocrine signal of nutritional stress in mice and humans. *Cell Metab.* **29**, 707–718 (2019).
38. Kempf, T. et al. GDF-15 is an inhibitor of leukocyte integrin activation required for survival after myocardial infarction in mice. *Nat. Med.* **17**, 581–588 (2011).
39. Patsalos, A. et al. A growth factor-expressing macrophage subpopulation orchestrates regenerative inflammation via GDF-15. *J. Exp. Med.* **219**, e20210420 (2022).
40. Strelau, J. et al. Progressive postnatal motoneuron loss in mice lacking GDF-15. *J. Neurosci.* **29**, 13640–13648 (2009).
41. Di Liberto, G. et al. Neurodegenerative phagocytes mediate synaptic stripping in Neuro-HIV. *Brain* **145**, 2730–2741 (2022).
42. Wang, D. et al. GDF15 promotes weight loss by enhancing energy expenditure in muscle. *Nature* **619**, 143–150 (2023).
43. Cimino, I. et al. Activation of the hypothalamic–pituitary–adrenal axis by exogenous and endogenous GDF15. *Proc. Natl Acad. Sci. USA* **118**, e2106868118 (2021).
44. Sjøberg, K. A. et al. GDF15 increases insulin action in the liver and adipose tissue via a β-adrenergic receptor-mediated mechanism. *Cell. Metab.* **35**, 1327–1340 (2023).
45. Ley, K., Laudanna, C., Cybulsky, M. I. & Nourshargh, S. Getting to the site of inflammation: the leukocyte adhesion cascade updated. *Nat. Rev. Immunol.* **7**, 678–689 (2007).
46. Carrette, F. & Surh, C. D. IL-7 signaling and CD127 receptor regulation in the control of T cell homeostasis. *Semin. Immunol.* **24**, 209–217 (2012).
47. Zimmermann, R. et al. Fat mobilization in adipose tissue is promoted by adipose triglyceride lipase. *Science* **306**, 1383–1386 (2004).

48. Yamauchi, T., Iwai, M., Kobayashi, N. & Shimazu, T. Noradrenaline and ATP decrease the secretion of triglyceride and apoprotein B from perfused rat liver. *Pflügers Arch.* **435**, 368–374 (1998).
49. Globig, A. -M. et al. The β_1-adrenergic receptor links sympathetic nerves to T cell exhaustion. *Nature* **622**, 383–392 (2023).
50. Frikke-Schmidt, H. et al. GDF15 acts synergistically with liraglutide but is not necessary for the weight loss induced by bariatric surgery in mice. *Mol. Metab.* **21**, 13–21 (2019).
51. Madisen, L. et al. A robust and high-throughput Cre reporting and characterization system for the whole mouse brain. *Nat. Neurosci.* **13**, 133–140 (2010).
52. Roth, B. L. DREADDs for neuroscientists. *Neuron* **89**, 683–694 (2016).
53. Zhu, H. et al. Cre-dependent DREADD (designer receptors exclusively activated by designer drugs) mice. *Genesis* **54**, 439–446 (2016).
54. Eisenstein, A. et al. Activation of the transcription factor NRF2 mediates the anti-inflammatory properties of a subset of over-the-counter and prescription NSAIDs. *Immunity* **55**, 1082–1095 (2022).
55. Reyes, J., Zhao, Y., Pandya, K. & Yap, G. S. Growth differentiation factor-15 is an IFN-γ regulated mediator of infection-induced weight loss and the hepatic FGF21 response. *Brain Behav. Immun.* **116**, 24–33 (2024).
56. Benichou, O. et al. Discovery, development, and clinical proof of mechanism of LY3463251, a long-acting GDF15 receptor agonist. *Cell Metab.* **35**, 274–286 (2023).
57. Smith, W. B. et al. A growth differentiation factor 15 receptor agonist in randomized placebo-controlled trials in healthy or obese persons. *J. Clin. Endocrinol. Metab.* **110**, 771–786 (2024).
58. Melero, I. et al. Neutralizing GDF-15 can overcome anti-PD-1 and anti-PD-L1 resistance in solid tumours. *Nature* **637**, 1218–1227 (2024).
59. Ruud, L. E. et al. Activation of GFRAL+ neurons induces hypothermia and glucoregulatory responses associated with nausea and torpor. *Cell Rep.* **43**, 113960 (2024).
60. Korn, T. et al. Myelin-specific regulatory T cells accumulate in the CNS but fail to control autoimmune inflammation. *Nat. Med.* **13**, 423–431 (2007).
61. Luan, H. H. et al. GDF15 is an inflammation-induced central mediator of tissue tolerance. *Cell* **178**, 1231–1244 (2019).
62. Kressel, A. M. et al. Identification of a brainstem locus that inhibits tumor necrosis factor. *Proc. Natl Acad. Sci. USA* **117**, 29803–29810 (2020).
63. Chow, C. F. W. et al. Body weight regulation via MT1-MMP-mediated cleavage of GFRAL. *Nat. Metab.* **4**, 203–212 (2022).

[1]Institute of Neuroimmunology and Multiple Sclerosis, University Medical Center Hamburg-Eppendorf, Hamburg, Germany. [2]Hamburg Center for Translational Immunology, University Medical Center Hamburg-Eppendorf, Hamburg, Germany. [3]Experimental Tumor Immunology, Department of Obstetrics and Gynecology, University Hospital Würzburg, Würzburg, Germany. [4]Department of Pediatrics, Pediatric Rheumatology/Special Immunology, University Hospital Würzburg, Würzburg, Germany. [5]Department of Biochemistry and Molecular Cell Biology, University Medical Center Hamburg-Eppendorf, Hamburg, Germany. [6]Institute of Clinical Chemistry and Laboratory Medicine, University Medical Center Hamburg-Eppendorf, Hamburg, Germany. [7]Center for Thrombosis and Hemostasis (CTH), Johannes Gutenberg University Medical Center, Mainz, Germany. [8]Irish Centre for Vascular Biology, School of Pharmacy and Biomolecular Sciences, Royal College of Surgeons in Ireland, Dublin, Ireland. [9]Bio Innovation Hub Transformational Research Unit, Novo Nordisk, Boston, MA, USA. [10]Department of Surgery, University of Michigan, Ann Arbor, MI, USA. [11]Department of Obstetrics and Fetal Medicine, University Medical Center Hamburg-Eppendorf, Hamburg, Germany. [12]Department of Psychiatry and Medical Department, Campus Benjamin Franklin, Charité-Universitätsmedizin Berlin, Berlin, Germany. ✉e-mail: manuel.friese@zmnh.uni-hamburg.de

Methods

Participant cohorts

Indviduals with MS and healthy individuals were recruited through the MS outpatient clinic of the Department of Neurology, University Medical Center Hamburg-Eppendorf, and their blood samples were processed and stored by the Biobank of the Institute of Neuroimmunology and Multiple Sclerosis (Hamburger Patienteninformationssystem Multiple Sklerose, HAPIMS) approved by the local ethics committee (Hamburg Chamber of Commerce Act for the Health Professions, registration no. PV4405). Informed consent was obtained from all individuals. Blood samples were collected in polypropylene tubes (Sarstedt, S-Monovette, 7.5 ml; 01.1602) and processed within 2 h. The tubes were centrifuged at 1,840*g* for 10 min at 15 °C, and the supernatant was collected as serum. Pregnant women were recruited through the PRINCE (PRenatal IdeNtification of Children's HEalth) study, which enrolled women of legal age experiencing a singleton pregnancy during their first trimester (gestational weeks 12–14). These participants were subsequently invited to attend two additional prenatal visits during the second trimester (gestational weeks 24–26) and third trimester (gestational weeks 34–36). Women with chronic infections (such as HIV and hepatitis B/C), known substance abuse issues or pregnancies resulting from assisted reproductive technologies were not eligible for participation. All participants provided informed consent, and the study protocol received approval from the ethics committee of the Hamburg Chamber of Physicians (license no. PV3694). Serum samples of pregnant women who experienced miscarriage or performed elective abortion were collected during routine blood sampling and processed according to standard laboratory methods at the Laboratory for Pediatric Rheumatology/Special Immunology at the University Hospital Wuerzburg (ethics protocol nos. 28/08 and 239/10). The study adhered to the principles outlined in the Declaration of Helsinki for medical research involving human participants. Blood was collected in polystyrene tubes and allowed to coagulate for 45 min. The samples were centrifuged at 1,500*g* for 20 min at 4 °C within 60 min of collection. All serum samples were aliquoted and stored at −80 °C until further analysis. The characteristics of the participants are shown in Supplementary Tables 1–4.

Mice

All mice (C57BL/6J and BALB/c wild-type purchased from Charles River; *Gdf15*$^{-/-}$[40]; *Gfral*$^{-/-}$[50], *Gfral*-Cre[23] (purchased from the Jackson Laboratory, 036750), Ai14[51], LSL-hM3Dq-DREADD[53], *Gfral*-Cre × Ai14, *Gfral*-Cre × LSL-hM3Dq-DREADD and *Adrb2*$^{-/-}$[64] were kept under specific pathogen-free conditions in the central animal facility of the University Medical Center Hamburg-Eppendorf. Adult mice (6–20 weeks old) from both sexes were used, unless otherwise stated; mice were sex and age matched in all experiments. The mice were kept in a 12-h light–dark diurnal cycle, at 22°C ± 2 °C and 40–60% humidity, and given ad libitum access to standard chow (Altromin, 1328P) and water, unless otherwise stated. EAE mice additionally received DietGel Recovery (Ssniff; H007-72065). All animal care and experimental procedures were conducted in accordance with institutional guidelines and met the requirements of the German legal authorities. Ethical approvals were obtained from the State Authority of Hamburg, Germany (approval nos. 45/17, 007/22 and 108/24).

EAE

Mice were immunized subcutaneously with 200 µg $MOG_{35–55}$ peptide (peptides&elephants) in complete Freund's adjuvant (BD Difco, 263.910) containing 2 mg ml^{-1} *Mycobacterium tuberculosis* (BD Difco, 231.141). Additionally, 300 ng of pertussis toxin (Merck Millipore, 516560-50UG) was injected intraperitoneally on the day of immunization and again 2 days later. Animals were scored daily for clinical signs using the following system: 0, no clinical deficits; 1, tail weakness; 2, hind limb paresis; 3, partial hind limb paralysis; 3.5, full hind limb paralysis; 4, full hind limb paralysis and fore limb paresis; 5, premorbid or dead. Animals reaching a clinical score ≥ 4 or not recovering from hind limb paralysis for more than 7 consecutive days were euthanized according to the regulations of the local Animal Welfare Act. For the analysis of chronic EAE (>day 15 after immunization), the clinical disease score for animals excluded from the analysis due to disease severity was carried forward as the mean of the group for statistical analysis. The cumulative clinical score represents the sum of the daily scores assigned to an animal over time. Whenever possible, mice were randomly assigned to treatment groups (rAAV, recombinant GDF-15) and mice from different experimental groups were housed together to minimize bias due to cage effects. Investigators were blinded to the genotype, the injected rAAV and treatment in the EAE experiments. For treatment with native human GDF-15 (Novo Nordisk), the protein was diluted in 0.9% NaCl, and mice received daily subcutaneous injections of 5 nmol per kg of body weight at a zeitgeber time of 2 ± 1. Control animals received a solution of 0.5 mM sodium acetate and 0.225% glycerol in 0.9% NaCl as a vehicle control. For DREADD activation, mice received 4 µg ml^{-1} CNO dihydrochloride (Cayman, 25780) in drinking water starting 3 days before EAE induction. Water was replaced every day, and consumption was monitored throughout the experiment.

Viral injections

rAAVs were produced at the UKE vector facility using the PHP.eB capsid due to its high transduction efficacy in the CNS[65]. pUCmini-iCAP-PHP.eB was a gift from V. Gradinaru (Addgene plasmid, 103005). Viral genomes were determined by RT–qPCR using primers targeting the WPRE region. Mice were anesthetized with inhaled isoflurane (2–3%), and rAAVs were administered in 100 µl PBS by retrobulbar injection. Each mouse received a dose of 1×10^{11} viral genomes. Full transgene expression was observed 2 to 3 weeks after injection.

Flow cytometric nucleus sorting

Isolation of nuclei from mouse spinal cords was performed as previously described[66]. Briefly, mice were euthanized with CO_2 and perfused with cold PBS. Spinal cords were dissected and stored at −80 °C. The tissue was mechanically dissociated with a scalpel, added to 2 ml of EZ buffer (Sigma-Aldrich, NUC101) and dissociated using a glass douncer (Sigma-Aldrich, D9063). After a 5-min incubation on ice, the nuclei were pelleted by centrifugation (500*g*, 5 min, 4 °C) and the pellet was washed in 2 ml of EZ buffer, followed by two washing steps in nuclei incubation buffer (340 mM sucrose, 2 mM $MgCl_2$, 25 mM KCl, 65 mM glycerophosphate, 5% glycerol, 1 mM EDTA, 1% bovine serum albumin or BSA). Nuclei were filtered through a 30-µm filter, followed by staining with AF647-labeled NeuN antibody and 0.25 µg ml^{-1} propidium iodide (BioLegend, 421301) as a DNA counterstain. NeuN$^+$ and NeuN$^-$ single nuclei were sorted using a BD FACSAria III cell sorter (BD Biosciences) with a 70-µm nozzle. RNA for real-time PCR was isolated as described below.

Flow cytometric cell sorting

For isolation of astrocytes and immune cells from spinal cord tissue, we adapted a protocol by Scheyltjens et al.[67], incorporating the transcriptional inhibitor actinomycin D (ActD) throughout the workflow. Spinal cord tissue from EAE animals and healthy controls was collected in RPMI-1640 medium (PAN Biotech, P04-18500) supplemented with 25 mM HEPES (Gibco, 15630056) and 30 µM ActD (Cell Signaling, 15021S) after transcardial PBS perfusion. Tissue was dissociated into single-cell suspensions in 1 mg ml^{-1} collagenase A (Roche, 11088793001) and 200 IU ml^{-1} DNase I (Merck Millipore, 260913) using the gentleMACS Octo Dissociator (Miltenyi Biotec, program: Multi_F). The dissociated tissue was applied to a 70-µm cell strainer, and the filter was rinsed three times with RPMI-1640 supplemented with 25 mM HEPES and 3 µM ActD. Dissociated tissue was collected after centrifugation at 500*g* for 5 min at 4 °C, and immune and glial cells were enriched using

a discontinuous density gradient with Percoll PLUS (GE Healthcare, 17-5445-01). Isotonic Percoll solutions were prepared with HBSS and supplemented with 3 µM ActD. After centrifugation at 1,350*g* and 4 °C for 30 min, cells were collected from the interphase between the 30% Percoll and 70% Percoll layer. Cells were washed in FACS buffer (PBS, 1 mM EDTA, 1% BSA (Miltenyi Biotec, 130-091-376), 10 mM HEPES) at 650*g* and 4 °C for 10 min. Nonspecific Fc receptor-mediated antibody binding was blocked by pre-incubation with TruStain FcX anti-mouse CD16/CD32 antibody (BioLegend, 101320) for 10 min at 4 °C before staining with surface antibodies in FACS buffer for 20 min at 4 °C. All antibodies used in this study are listed in Supplementary Table 7. Cells were washed and resuspended in FACS buffer supplemented with 0.4 U µl^{-1} RiboLock RNase Inhibitor (Thermo Fisher Scientific, EO0382) and 2.5 µM Helix NP Green (BioLegend, 425303) to exclude dead cells. Up to 70,000 cells were sorted into DNA LoBind tubes (Eppendorf, 0030108051) filled with 700 µl RLT buffer supplemented with 40 mM dithiothreitol (Roche, 10197777001) using a BD FACSAria III cell sorter (BD Biosciences) equipped with a 100-µm nozzle. RNA for real-time PCR was processed as described below.

Real-time PCR

RNA was extracted using the RNeasy Mini Kit (Qiagen) with DNase I treatment and subsequently reverse-transcribed to complementary DNA using the RevertAid H Minus First Strand cDNA Synthesis Kit (Thermo Fisher Scientific) according to the manufacturer's instructions. Gene expression was analyzed by the QuantStudio Flex 6 Real-Time PCR System (Applied Biosystems) using TaqMan Gene Expression Assays (Thermo Fisher Scientific) for *Gdf15* (Mm00442228_m1), *Tbp* (Mm01277042), *Adrb1* (Mm00431701_s1), *Adrb2* (Mm02524224_s1) and *Adrb3* (Mm00442669_m1) or PowerUp SYBR Green Master Mix (Applied Biosystems) using custom-made oligonucleotides for *Gfral* and *Tbp* (Supplementary Table 8). Primer design was performed using a built-in algorithm in Benchling. All analyses were performed in technical duplicates or triplicates. We calculated gene expression as $2^{-\Delta Ct}$ relative to *Tbp* as the endogenous control.

Cell lines

Neuro-2a cells and HEK 293T cells were obtained from DSMZ (ACC 148) and passaged in DMEM high glucose (Gibco, 61965059) supplemented with 10% fetal bovine serum (Pan Biotech, P30-3306) and 1% penicillin–streptomycin (Gibco, 15070063). SIM-A9 microglial cells were obtained from Biocat (T0247-GVO-ABM) and passaged in DMEM:F12 (Pan Biotech, P04-41250) supplemented with 10% heat-inactivated fetal bovine serum (Sigma-Aldrich, F7524), 5% heat-inactivated horse serum (Pan Biotech, P30-0702) and 1% penicillin–streptomycin. All cell lines were maintained at 37 °C and 5% CO_2, and regularly checked for mycoplasma contamination using the VenorGeM Advance kit (Minerva Biolabs, 11-7024) according to the manufacturer's instructions. To generate stable cell lines expressing the *Gdf15*-mScarlet reporter construct, Neuro-2a and SIM-A9 microglial cells were transduced with lentiviral particles in the presence of 8 µg ml^{-1} polybrene (Sigma-Aldrich, H9268), and mScarlet$^+$ cells were isolated using a BD FACSAria III cell sorter. Samples were supplemented with 10 µM DAPI (BioLegend, 422801) before acquisition to exclude dead cells.

Primary neuronal and astrocytic cultures

For primary cortical cultures, pregnant C57BL/6J mice were euthanized at gestational day 15.5. The cortex was isolated and dissociated, and cells were plated at a density of 6×10^4 per cm^2 on poly-D-lysine-coated wells (5 µM, Sigma-Aldrich, P6407). For immunocytochemistry, primary cortical neurons and astrocytes were cultivated on poly-D-lysine-coated 12-mm diameter coverslips. Unless otherwise stated, cells were maintained in Neurobasal Plus medium (supplemented with B-27 Plus, penicillin, streptomycin, and L-glutamine; Gibco, A3582901) at 37 °C and 5% CO_2, and a relative humidity of 98%. Half-medium exchanges were performed every 3 to 4 days. Throughout this study, cultures after 14 to 18 days in vitro were used for experiments.

Primary T cell cultures

For primary T cell cultures, spleens and lymph nodes from C57BL/6J mice were collected and processed into a single-cell suspension using 70-µm cell strainers. Red blood cells in splenocytes were lysed by incubation in erythrocyte lysis buffer (10 mM potassium bicarbonate, 0.15 M ammoniochloride, 0.1 mM Na_2EDTA in double-distilled water; pH 7.4) for 2 min. Spleen and lymph node cells were pooled, and T cells were enriched using the MojoSort Mouse CD3 or CD4 T cell Isolation Kit (BioLegend, 480024 or 480006, respectively) according to the manufacturer's instructions. Flat-bottom cell culture plates were coated with 0.5 µg ml^{-1} anti-CD3 (BioLegend, 100238), and cells were seeded in T cell medium (RPMI-1640, 10% heat-inactivated fetal bovine serum, 1% penicillin–streptomycin, 10 mM HEPES, 50 µM 2-mercaptoethanol (Gibco, 31350010), 1% GlutaMAX (Gibco, 35050061), 1 mM sodium pyruvate (Gibco, 11360070) and 1% non-essential amino acids (Gibco, 11140050)) supplemented with 0.5 µg ml^{-1} anti-CD28 (BioLegend, 102116) and 25 IU ml^{-1} recombinant mouse IL-2 (PeproTech, 212-12). For proliferation assays, T cells were stained with 5 µM CellTrace CFSE (Invitrogen, C34554) before seeding according to the manufacturer's instructions.

Compounds and chemicals

Compounds were added to primary cells or cell lines at the indicated time points specified in the respective figure legends. Unless otherwise stated, cells were stimulated every 24 h. The following concentrations were used: 20 or 100 ng ml^{-1} recombinant mouse IFNγ (PeproTech, 315-05), 20 ng ml^{-1} recombinant mouse GM-CSF (PeproTech, 315-03), 1 µg ml^{-1} tunicamycin (Sigma-Aldrich, T7765), 250 µg ml^{-1} 4-ocytl itaconate (Hycultec, HY-112675), 10 µM norepinephrine (Cayman, Cay16673), 10 µM epinephrine (Sigma-Aldrich, E4250), 10 µM xamoterol (Cayman, Cay24267), 10 µM indacaterol (Cayman, Cay20070), 10 µM CGP 20712A (Cayman, Cay40765-1), 10 µM ICI 118551 (Hycultec, HY-13951), 100 ng ml^{-1} lipopolysaccharide (Sigma-Aldrich, L4391) and 10 ng ml^{-1} or 50 ng ml^{-1} native human GDF-15 (Novo Nordisk).

Immunocytochemistry, immunohistochemistry and imaging

Cells were fixed with 4% paraformaldehyde and incubated in 5% normal donkey serum (NDS) containing 0.1% Triton X-100. Immunolabeling was performed in 2% NDS and 1% BSA in 0.1% Triton X-100. All antibodies used in this study and their dilutions are provided in Supplementary Table 7. Images were acquired using a confocal LSM 900 laser scanning confocal microscope (Zeiss). We quantified the endogenous intracellular mScarlet signal in neurons (NeuN$^+$) and astrocytes (GFAP$^+$) using ImageJ 1.54i. For each biological replicate, we calculated the mean from three regions of interest per coverslip. Mouse spinal cord, brain and spleen tissue were obtained and processed as described previously[68]. Briefly, cryosections from perfused and paraformaldehyde-fixed mid-cervical spinal cords, brain or spleen were incubated in 5% NDS containing 0.1% Triton X-100 and were subsequently stained with antibodies listed in Supplementary Table 7. For antibodies of mouse origin, sections were additionally incubated with AffiniPure Fab fragment donkey anti-mouse IgG (H+L; Jackson ImmunoResearch) for 60 min at room temperature. Images were acquired using an LSM 900 laser scanning confocal microscope (Zeiss) and analyzed using ImageJ 1.54i. For the quantification of Iba1 and GFAP, a mask for the gray matter or white matter was manually applied, and the MFI was calculated for each region of interest. For the quantification of absolute cell counts (CD45, CD68, CD3), all positive cells per spinal cord section were counted. During quantification in Fiji, the investigators were blinded to the experimental group.

Immune cell isolation for flow cytometry

iLNs and spleen samples were homogenized through a 70-µm cell strainer and washed with PBS (500*g*, 5 min, 4 °C). Red blood cells

were lysed as described above. Brain and spinal cord tissue were collected after transcardial PBS perfusion and dissociated into single-cell suspensions in 1 mg ml^{-1} collagenase A and 0.1 mg ml^{-1} DNase I using the gentleMACS Octo Dissociator (program: Multi_F). The dissociated tissue was applied to a 70-µm cell strainer, and immune and glial cells were enriched using a discontinuous density gradient (GE Healthcare, GE17-0891-01). Cells were collected from the interphase as described above. Nonspecific Fc receptor-mediated antibody binding was blocked by pre-incubation with TruStain FcX anti-mouse CD16/CD32 antibody before staining of surface antibodies in Brilliant Stain Buffer (BD Biosciences) for 30 min at 4 °C. For staining of intranuclear proteins cells were fixed in 1× Fixation/Permeabilization working solution for 45 min at 4 °C, followed by incubation with antibodies targeting Nur77 or Ki67 in 1× Permeabilization buffer for 45 min at 4 °C (Invitrogen, 00-5523). All antibodies used in this study are listed in Supplementary Table 7. We excluded dead cells from the analysis by staining with Zombie Aqua, Green, Yellow and NIR Fixable Viability Stains (BioLegend, 423101, 423112, 423104, 423106) or 0.8 µM Alexa Fluor 750 NHS (Invitrogen, A20011). For the determination of absolute cell numbers, $CD45^{hi}$ leukocytes and $CD45^{int}$ microglia were quantified using Precision Count Beads (BioLegend, 424902). Data were obtained using a BD Symphony A3 flow cytometer (BD Biosciences) and analyzed using FlowJo version 10.9 (BD Biosciences). During the analysis in FlowJo, the investigators were blinded to the experimental group.

RNA sequencing and analysis

RNA was isolated from $CD4^+$ enriched T cells using the RNeasy Mini Kit (Qiagen) with DNase I treatment. RNA-sequencing libraries were prepared using the TruSeq stranded mRNA Library Prep Kit (Illumina) according to the manufacturer's instructions. Libraries were pooled and sequenced on a NovaSeq 6000 sequencer (Illumina), generating 150-base-pair, paired-end reads with poly-A enrichment. The reads were aligned to the Ensembl mouse reference genome (GRCh39) using STAR v2.7.9a with default parameters for paired-end reads. Gene assignments were quantified with featureCounts v1.5.1. Differential expression analysis used DESeq2 v1.40.2 with an FDR-adjusted significance threshold of $P < 0.05$. Differentially expressed genes were annotated using biomaRt v2.56.1. Sample similarity was assessed through principal component analysis utilizing the top 500 genes with the highest variance of $\log_2$-normalized counts. Gene expression heat maps and visualizations were generated with ggplot2 v3.4.3 for comprehensive data representation.

Immunoblot

Tissue from EAE and healthy mice were homogenized in radioimmunoprecipitation buffer (50 mM Tris, 150 mM NaCl, 0.5 mM EDTA, 10% SDS, 1% NP-40, 10% sodium deoxycholate, plus protease and phosphate inhibitor cocktails (PhosSTOP Merck, 4906845001 and cOmplete, Sigma-Aldrich, 11836170001)) using a Qiagen TissueLyser LT with the setting 1/50s for 1 min and incubated at 4 °C for 30 min on a rotating wheel. The lysates were centrifuged for 10 min at 16,000*g* to remove the cell debris. Protein concentrations were determined by BCA assay (Pierce BCA Protein Assay Kit, Thermo Fisher Scientific, 23228 and 23224) according to the manufacturer's protocol. Samples were prepared using Western-Ready Protein Sample Loading Buffer (5×; BioLegend, 426311) and boiled at 95 °C for 10 min. A total of 10 µg of protein was loaded onto 8–12% gradient or 10% non-gradient SDS–PAGE (NuPAGE, Thermo Fisher Scientific, NW04125BOX, NW00105BOX) followed by wet transfer to polyvinylidene fluoride membranes. Blocking was performed using 5% milk powder in 1× TBS-T for 1 h at room temperature. Membranes were incubated with primary antibodies overnight at 4 °C. Horseradish peroxidase-coupled secondary antibodies were applied for 1 h at room temperature, and chemiluminescence was visualized using WesternSure PREMIUM Chemiluminescent Substrate (LI-COR, 926-95000) according to the manufacturer's protocol. All antibodies used are listed in Supplementary Table 7.

Statistics and reproducibility

The statistical analyses applied during the bioinformatics analysis are detailed in the respective sections. Unless otherwise stated, the data are presented as means ± s.e.m. or the mean alone if individual data points for biological replicates are displayed. Data distribution was assumed to be normal, but this was not formally tested. All statistical analyses were performed using Prism 9.5.1 (GraphPad) as indicated in the figure legends. Corrections for multiple testing were controlled by the FDR (Benjamini and Hochberg). A P value of ≤0.05 was considered significant.

To determine sample sizes, we performed a power analysis using G*Power 3.1 with the following parameters based on previous studies[66,68] and existing preliminary data: two-sided Wilcoxon–Mann–Whitney test; type I error, 0.05; type II error, 0.2; effect size based on Cohen, 1 to 2.5 (varies between experimental setups).

Whenever immunohistochemical stainings of reporter mice are shown, we analyzed sections from at least three individual animals and selected representative images.

Reporting summary

Further information on research design is available in the Nature Portfolio Reporting Summary linked to this article.

Data availability

Sequencing data generated for this study have been deposited in the Gene Expression Omnibus under accession code GSE288193. All other data are available in the main text or the Supplementary Information. Source data are provided with this paper.

Code availability

The code used for the study can be obtained from the corresponding author upon reasonable request.

References

64. Rohrer, D. K., Chruscinski, A., Schauble, E. H., Bernstein, D. & Kobilka, B. K. Cardiovascular and metabolic alterations in mice lacking both β1- and β2-adrenergic receptors. *J. Biol. Chem.* **274**, 16701–16708 (1999).
65. Chan, K. Y. et al. Engineered AAVs for efficient noninvasive gene delivery to the central and peripheral nervous systems. *Nat. Neurosci.* **20**, 1172–1179 (2017).
66. Rothammer, N. et al. G9a dictates neuronal vulnerability to inflammatory stress via transcriptional control of ferroptosis. *Sci. Adv.* **8**, eabm5500 (2022).
67. Scheyltjens, I. et al. Single-cell RNA and protein profiling of immune cells from the mouse brain and its border tissues. *Nat. Protoc.* **17**, 2354–2388 (2022).
68. Schattling, B. et al. TRPM4 cation channel mediates axonal and neuronal degeneration in experimental autoimmune encephalomyelitis and multiple sclerosis. *Nat. Med.* **18**, 1805–1811 (2012).

Acknowledgements

We thank the Friese laboratory for discussions. We thank the UKE vector facility for supplying viral vectors and for technical advice. We acknowledge the support from the Team of the Biobank of the Institute of Neuroimmunology and Multiple Sclerosis (INIMS) and of the PRINCE study for their support in participant sample processing. We thank A. Zenclussen (Department of Environmental Immunology, Helmholtz Centre for Environmental Research, Leipzig, Germany) for providing serum samples from pregnant women. We thank J. Strelau (Department of Functional Neuroanatomy, University of

Heidelberg, Heidelberg, Germany) for providing *Gdf15*$^{-/-}$ animals, C. E. Gee (Institute for Synaptic Neuroscience, ZMNH, University Medical Center Hamburg-Eppendorf, Hamburg, Germany) for providing LSL-hM3Dq-DREADD animals, O. Ohana for providing Ai14 animals (Institute for Molecular and Cellular Cognition, ZMNH, University Medical Center Hamburg-Eppendorf, Hamburg, Germany) to generate GFRAL reporter animals, and J. Keller and A. Baranowsky (Department of Trauma and Orthopaedic Surgery, University Medical Center Hamburg-Eppendorf, Hamburg, Germany) for providing *Adrb2*$^{-/-}$ animals. We acknowledge the technical support from T. Andreas (Department of Obstetrics and Fetal Medicine, University Medical Center Hamburg-Eppendorf, Hamburg, Germany), A. Coneva, V. Telmon, A. Hartmann and H. Höhnke (Institute of Neuroimmunology and Multiple Sclerosis, University Medical Center Hamburg-Eppendorf, Hamburg, Germany).

This work was funded by the Deutsche Forschungsgemeinschaft (DFG, German Research Foundation) – KFO 296 (255154572 to M.A.F., S.M.G., A.D. and P.A.); SFB 1713 (534829736 to J.K.S., A.D., P.C.A, S.M.G., J.H. and M.A.F.); FOR 2879 (405358801 to M.A.F.); FOR 5705 (523862973 to J.B.E. and M.A.F.) – the Bundesministerium für Bildung und Forschung (01KT2310 to J.W.), TRANSCAN (ERA-NET – JTC 2021, iParaCyts to J.W.), the Else Kröner-Fresenius Stiftung (EKEA.198 to J.K.S.) and the Werner Otto-Stiftung (07/104 to J.K.S.). J.B.E. is supported by the Hertie Network of Excellence in Clinical Neuroscience (P1200009).

Author contributions

J.K.S. and M.A.F. designed the study. J.K.S., A. Kahn and M.A.F. planned most experiments. J.K.S., L.B.-L. and C.R. conducted bioinformatical analyses. L.B.-L. illustrated the graphical summary. J.K.S. and A. Kahn performed and analyzed most in vitro and in vivo experiments with additional contributions from L.B.-L., J.B.E., B.H., C.Z., L.U., S.B., F.F., G.A., M.W., C.M., A. Kolakowska, S.G., I.W., N.R., M.H., V.H.-v.d.S., V.T., V.V. and N.M. T.R., M.P., S.B.J., R.J.S., A.D., P.C.A., S.M.G., J.H. and J.W. provided material and expertise. J.K.S., A. Kahn and M.A.F. wrote the initial version of the manuscript. M.A.F. supervised and funded the study. All co-authors contributed to the editing and discussion of the manuscript and approved the final version.

Competing interests

S.B.J. is an employee of Novo Nordisk, a pharmaceutical company producing and selling medicine for the treatment of diabetes and obesity. R.J.S. has received research support from Novo Nordisk, Fractyl, Astra Zeneca, Congruence Therapeutics, Eli Lilly, Bullfrog AI, Glyscend Therapeutics and Amgen. R.J.S. has served as a paid consultant for Novo Nordisk, Eli Lilly, CinRx, Fractyl, Structure Therapeutics, Crinetics, Amgen, Congruence Therapeutics and Nuanced Health. R.J.S. has equity in Bullfrog AI, Nuanced Health, Coro Bio and Rewind. J.W. is an inventor on patents related to GDF-15 as a biomarker and therapeutic target in cancer, and a cofounder and shareholder of the biotech company CatalYm. The other authors declare no competing interests.

Additional information

Extended data is available for this paper at https://doi.org/10.1038/s41590-025-02406-1.

Supplementary information The online version contains supplementary material available at https://doi.org/10.1038/s41590-025-02406-1.

Correspondence and requests for materials should be addressed to Manuel A. Friese.

Peer review information *Nature Immunology* thanks Thomas Korn and the other anonymous reviewer(s) for their contribution to the peer review of this work. Primary Handling Editor: Nick Bernard, in collaboration with the *Nature Immunology* team.

https://doi.org/10.1038/s41590-025-02406-1

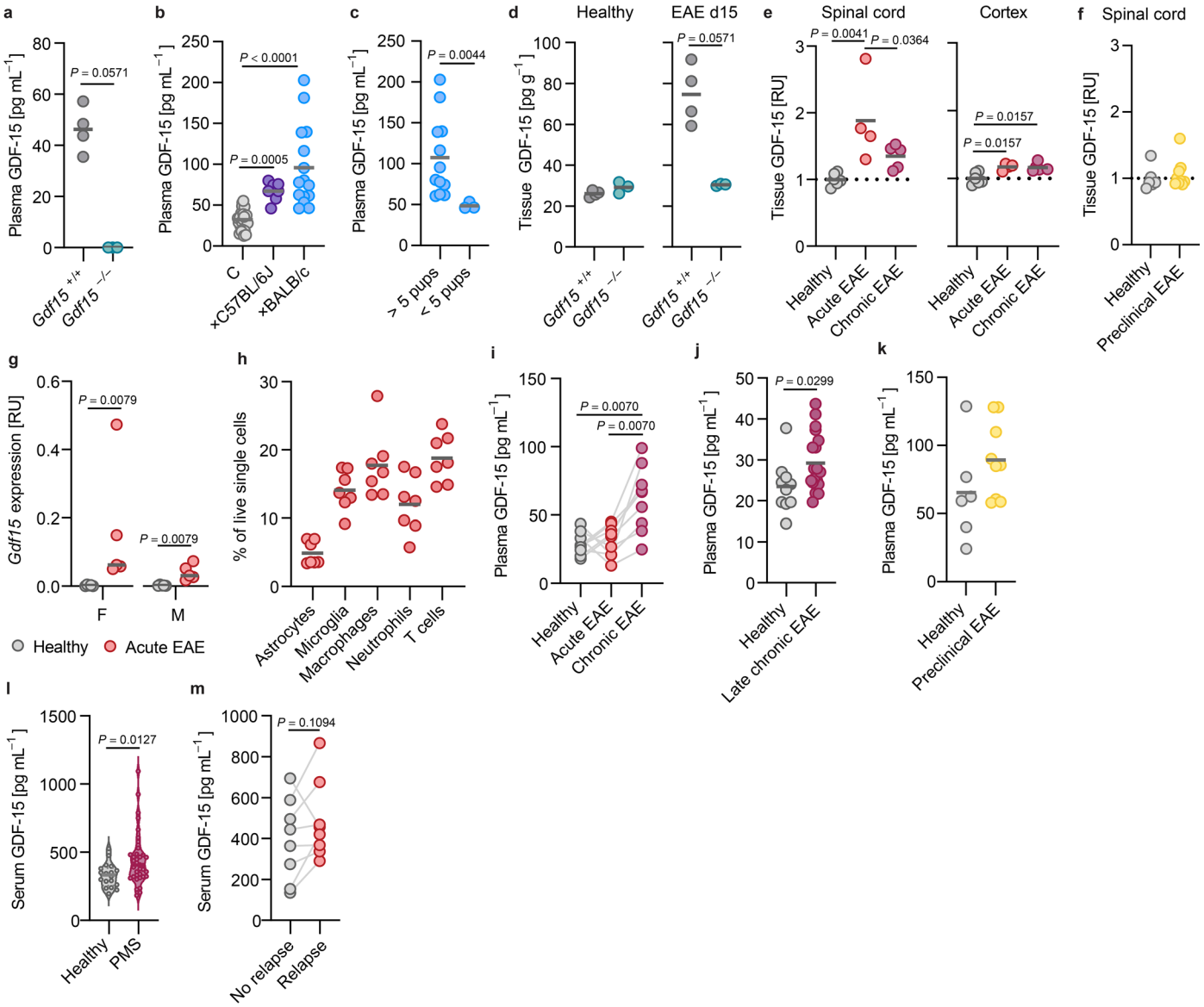

Extended Data Fig. 1 | Chronic CNS inflammation elevates peripheral GDF-15 levels. a-c, Plasma concentrations of GDF-15 in a, healthy female *Gdf15*$^{+/+}$ ($n = 4$) and *Gdf15*$^{-/-}$ ($n = 3$) littermates, **b**, female C57BL/6J mice from controls (C, $n = 23$), syngeneic matings (C57BL/6J, $n = 8$), or semi-allogeneic matings (BALB/c, $n = 15$) in trimester 3 (GD17.5 ± 1), and **c**, dams from semi-allogeneic matings in trimester 3, low ($n = 3$) and regular ($n = 12$) pup counts. **d**, Protein expression of GDF-15 in spinal cord measured by tissue lysate ELISA in healthy and acute EAE (day 15 post immunization (p.i.)) female *Gdf15*$^{+/+}$ mice and *Gdf15*$^{-/-}$ littermates; $n = 4$ for *Gdf15*$^{+/+}$, $n = 3$ for *Gdf15*$^{-/-}$. **e**, **f**, Relative protein levels of GDF-15 measured by tissue lysate ELISA in **e**, spinal cord and cortex of female healthy ($n = 6$), acute EAE (day 15 p.i., $n = 4$), or chronic EAE (day 30 p.i., $n = 5$) mice, and **f**, spinal cord of female healthy ($n = 6$) and preclinical EAE (day 9 p.i., $n = 9$) mice. **g**, *Gdf15* expression from spinal cord nonneuronal (NeuN$^-$) nuclei measured by RT-qPCR in female and male healthy and acute EAE mice (day 15/16 p.i.); $n = 5$ per group. **h**, Frequency of cell populations from Fig. 1g within viable single cells in acute EAE (day 15/16 p.i.) $n = 7$. **i-k**, Plasma concentrations of GDF-15 in **i**, female C57BL/6J mice before EAE induction, in the acute (day 14 p.i.) and chronic phases (day 29 p.i.) $n = 9$, **j**, late chronic EAE mice (day 59 p.i.; $n = 19$) and healthy littermate controls ($n = 10$) and **k**, preclinical EAE mice (day 9 p.i.; $n = 9$) and healthy littermate controls ($n = 6$). **l**, **m**, GDF-15 serum concentrations in **l**, progressive (PMS; $n = 36$) MS patients compared to healthy controls ($n = 18$) and **m**, relapse vs. non-relapse samples from the same MS patient; $n = 8$. Individual datapoints represent biological replicates. For (**a**, **c**, **d**, **f**, **g**, **h**, **k**, **l**) two-sided Mann-Whitney tests were performed. In (**b**, **e**), Kruskal-Wallis tests with FDR correction were performed. In (**i**), a Friedman test with FDR correction was used. For (**m**), a Wilcoxon test was used. RU = Relative units.

https://doi.org/10.1038/s41590-025-02406-1

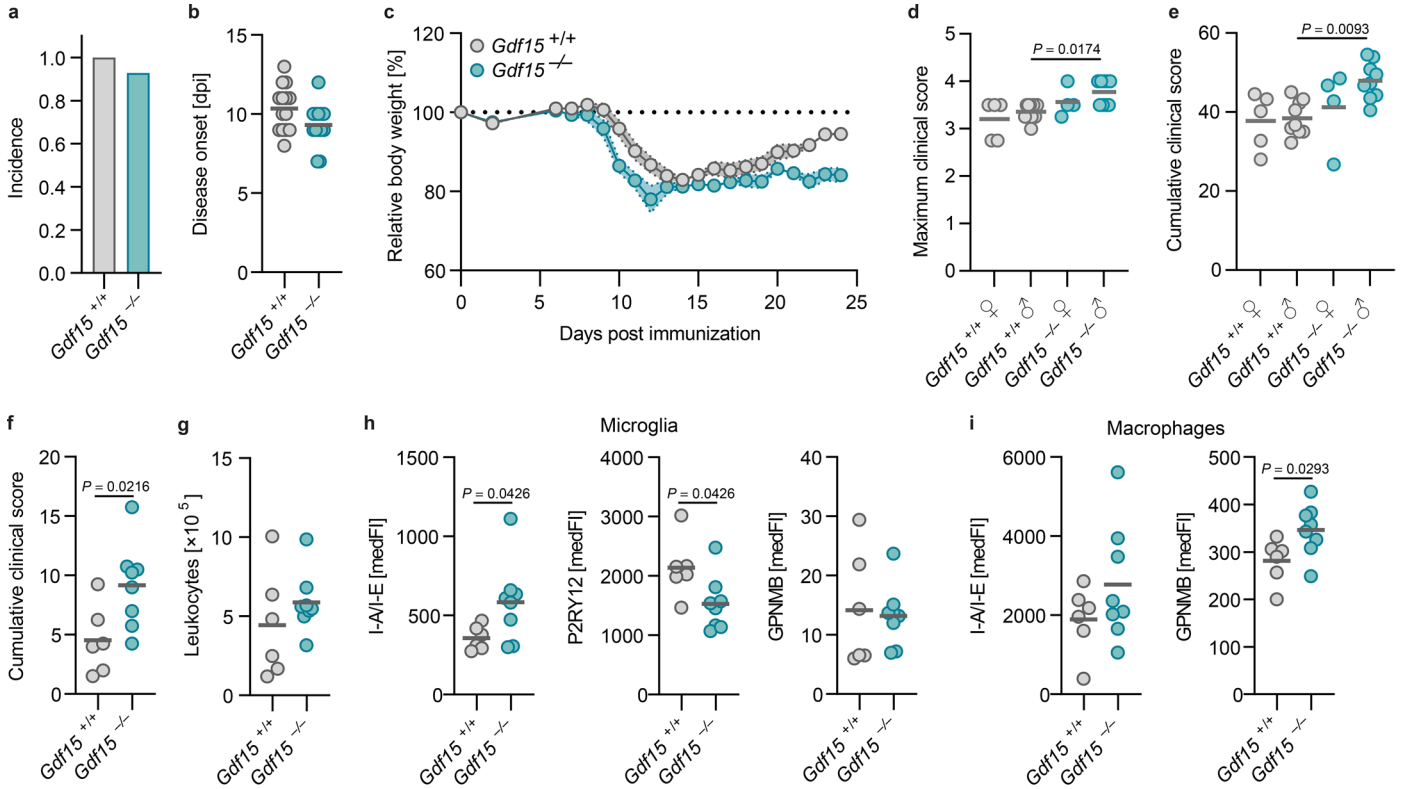

Extended Data Fig. 2 | *Gdf15* deletion exacerbates CNS inflammation. **a**-**e**, EAE was induced in *Gdf15*$^{+/+}$ ($n = 14$) and *Gdf15*$^{-/-}$ ($n = 13$) mice. **a**, Incidence, **b**, disease onset, and **c**, relative body weight loss. **d**, Maximum clinical score and **e**, cumulative clinical score in female and male *Gdf15*$^{+/+}$ and *Gdf15*$^{-/-}$ mice; $n = 9$ for males, $n = 5$ for *Gdf15*$^{+/+}$ females and $n = 4$ for *Gdf15*$^{-/-}$ females. **f**-**i**, Characterization of microglia and CNS-infiltrating immune cells during acute EAE (day 15 p.i.); $n = 6$ for *Gdf15*$^{+/+}$, $n = 8$ for *Gdf15*$^{-/-}$. **f**, Cumulative clinical score. **g**, Absolute number of viable leukocytes (CD45^{hi}). **h**, Median fluorescence intensity (medFI) of MHC II, P2RY12 and GPNMB on microglia. **i**, MedFI of MHC II and GPNMB on infiltrating macrophages. Individual datapoints represent biological replicates. Data are shown as mean ± s.e.m. (**c**). For (**a**), a Fisher's exact test was used. For (**d**, **e**), a Kruskal-Wallis test with FDR correction was performed. In (**b**, **f**-**i**), a two-sided Mann-Whitney test was performed. Dpi, days post immunization.

https://doi.org/10.1038/s41590-025-02406-1

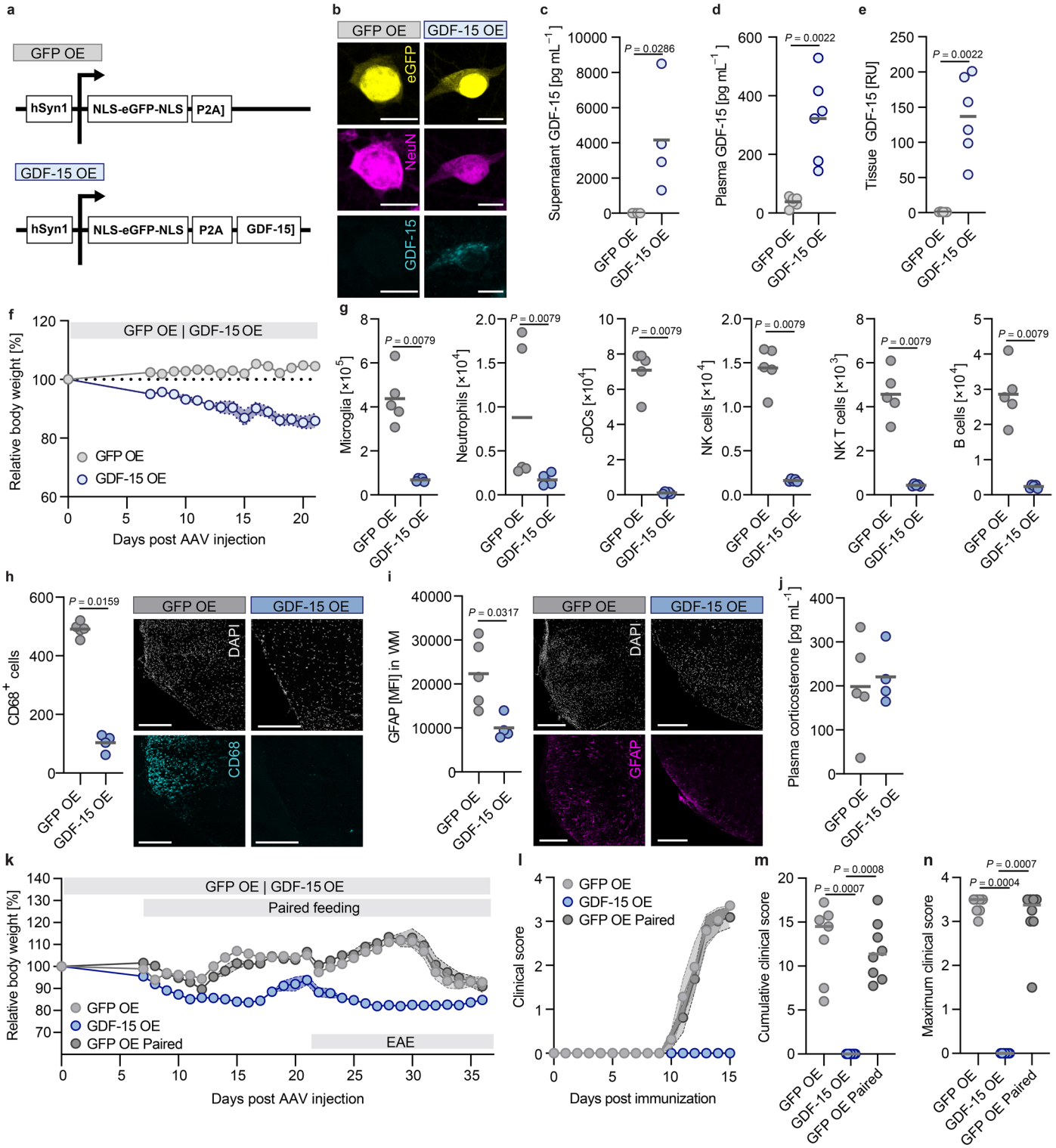

Extended Data Fig. 3 | See next page for caption.

https://doi.org/10.1038/s41590-025-02406-1

Extended Data Fig. 3 | Neuronal GDF-15 delivery induces body weight loss. **a**, Gene delivery construct. hSyn1, Human synapsin 1 promoter; NLS, nuclear localization sequence; P2A, peptide 2A cleavage site; closed reading frame. **b**, Staining of GDF-15 in primary cortical neurons transduced with an rAAV coding for eGFP (GFP OE) or mouse GDF-15 (GDF-15 OE) at a multiplicity of infection (MOI) of 20,000 on DIV7. Scale bars, 10 µm. **c**, GDF-15 concentration in supernatant from transduced primary cortical neurons; $n = 4$. **d**-**f**, Female C57BL/6J mice were injected with a GFP OE or GDF-15 OE rAAV; $n = 6$ per group. **d**, Plasma concentration and **e**, brain tissue concentration of GDF-15 on day 21 post-injection. **f**, Relative body weight change. **g**-**j**, Female C57BL/6J mice were injected with a GFP OE or GDF-15 OE rAAV prior to EAE induction. Analyses were performed in acute EAE (day 15 post immunization (p.i.)). **g**, Quantification of immune cell infiltrates in the brain and spinal cord in; $n = 5$ per group. **h**, Quantification of $CD68^+$ myeloid cells in cervical spinal cord sections; $n = 5$ for GFP OE, $n = 4$ for GDF-15 OE. Scale bars, 200 µm. **i**, Mean fluorescence intensity (MFI) of GFAP staining in the white matter (WM) of cervical spinal cord sections; $n = 5$ for GFP OE, $n = 4$ for GDF-15 OE. Scale bars, 200 µm. **j**, Plasma concentrations of corticosterone; $n = 5$ for GFP OE, $n = 4$ for GDF-15 OE. **k**-**n**, Female C57BL/6J mice were injected with a GFP OE or GDF-15 OE rAAV; $n = 7$ for GFP OE and GDF-15 OE, $n = 8$ for GFP OE Paired. **k**, Relative body weight loss, **l**, mean clinical disease score, **m**, cumulative disease score, and **n**, maximum disease score after EAE injection. Individual datapoints represent biological replicates. Data are shown as mean ± s.e.m. (**f**, **k**, **l**). For (**c**-**e**, **g**-**j**), two-sided Mann-Whitney tests were performed. For (**m**, **n**), a Kruskal-Wallis test with FDR correction was performed. OE, overexpression; RU, relative units.

https://doi.org/10.1038/s41590-025-02406-1

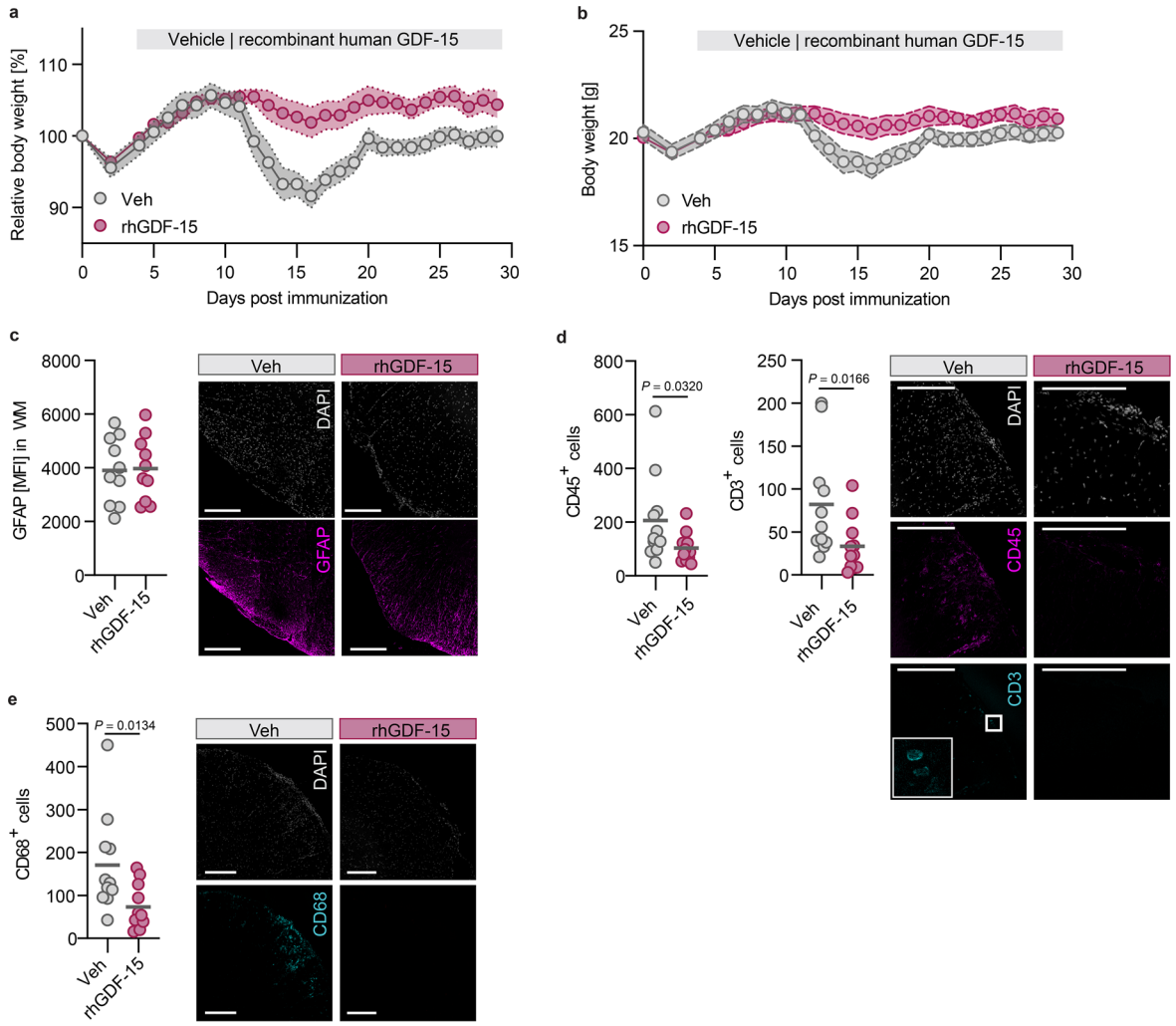

Extended Data Fig. 4 | Recombinant GDF-15 prevents immune cell infiltration. EAE was induced in female C57BL/6J mice, and animals received daily subcutaneous injections of 5 nmol per kg of body weight of recombinant human GDF-15 (rhGDF-15, $n = 12$) or a vehicle control (Veh, $n = 11$) from day 4 post immunization (p.i.) onwards. **a**, Relative body weight loss. **b**, Absolute body weight. **c**, Mean fluorescence intensity (MFI) of GFAP staining in the white matter (WM) of cervical spinal cord sections in chronic EAE (day 29 p.i.); $n = 10$ per group. Scale bars, 200 µm. **d**, Number of leukocytes ($CD45^+$) and T cells ($CD3^+$), and **e**, myeloid cells ($CD68^+$) in cervical spinal cord sections in chronic EAE (day 29 p.i.); $n = 11$ per group. Scale bars, 200 µm. Individual datapoints represent biological replicates. Data are shown as mean ± s.e.m. (**a**, **b**). For (**c**-**e**), two-sided Mann-Whitney test were performed.

https://doi.org/10.1038/s41590-025-02406-1

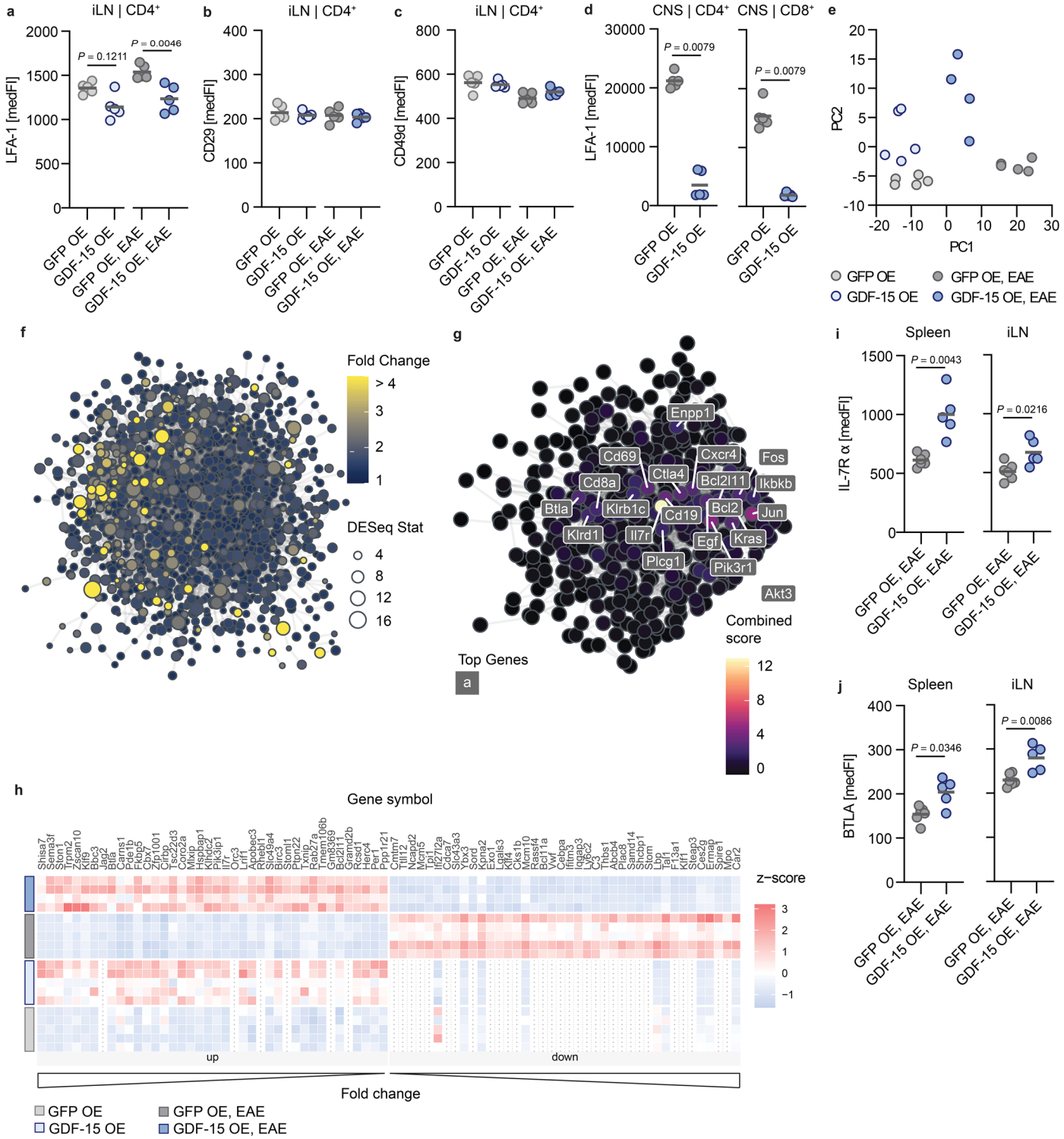

Extended Data Fig. 5 | GDF-15 delivery modulates CD4$^+$ T cell phenotype. Female C57BL/6J mice were injected with an rAAV coding for eGFP (GFP OE) or mouse GDF-15 (GDF-15 OE). In preclinical EAE groups, mice were immunized, and organs were collected on day 9 post immunization (p.i.) prior to disease onset. **a-c**, Median fluorescence intensity (medFI) of selected markers on CD4$^+$ T cells in the iLN; $n = 5$ per group. **d**, MedFI of LFA-1 on CD4$^+$ and CD8$^+$ T cells in the CNS during acute EAE (day 15 p.i.); $n = 5$ per group. **e-h**, Splenic CD4$^+$ T cells were purified and processed for mRNA sequencing; $n = 5$ per group. **e**, Principal component analysis. **f**, Fold change and statistics for KEGG pathway analysis between GFP OE, EAE and GDF-15 OE; EAE group. **g**, Top regulated genes in upper left cluster. **h**, Heatmap of differentially regulated genes. **i**,**j**, medFI of selected markers on CD4$^+$ T cells three weeks after rAAV injection on day 9 p.i.; $n = 5$ per group. **i**, Interleukin (IL)-7Rα in the spleen and inguinal lymph nodes (iLN). **j**, B lymphocyte and T lymphocyte attenuator (BTLA) in the spleen and iLN. Individual datapoints represent biological replicates. For (**a-d**, **i**, **j**), two-sided Mann-Whitney tests were performed. OE, overexpression.

https://doi.org/10.1038/s41590-025-02406-1

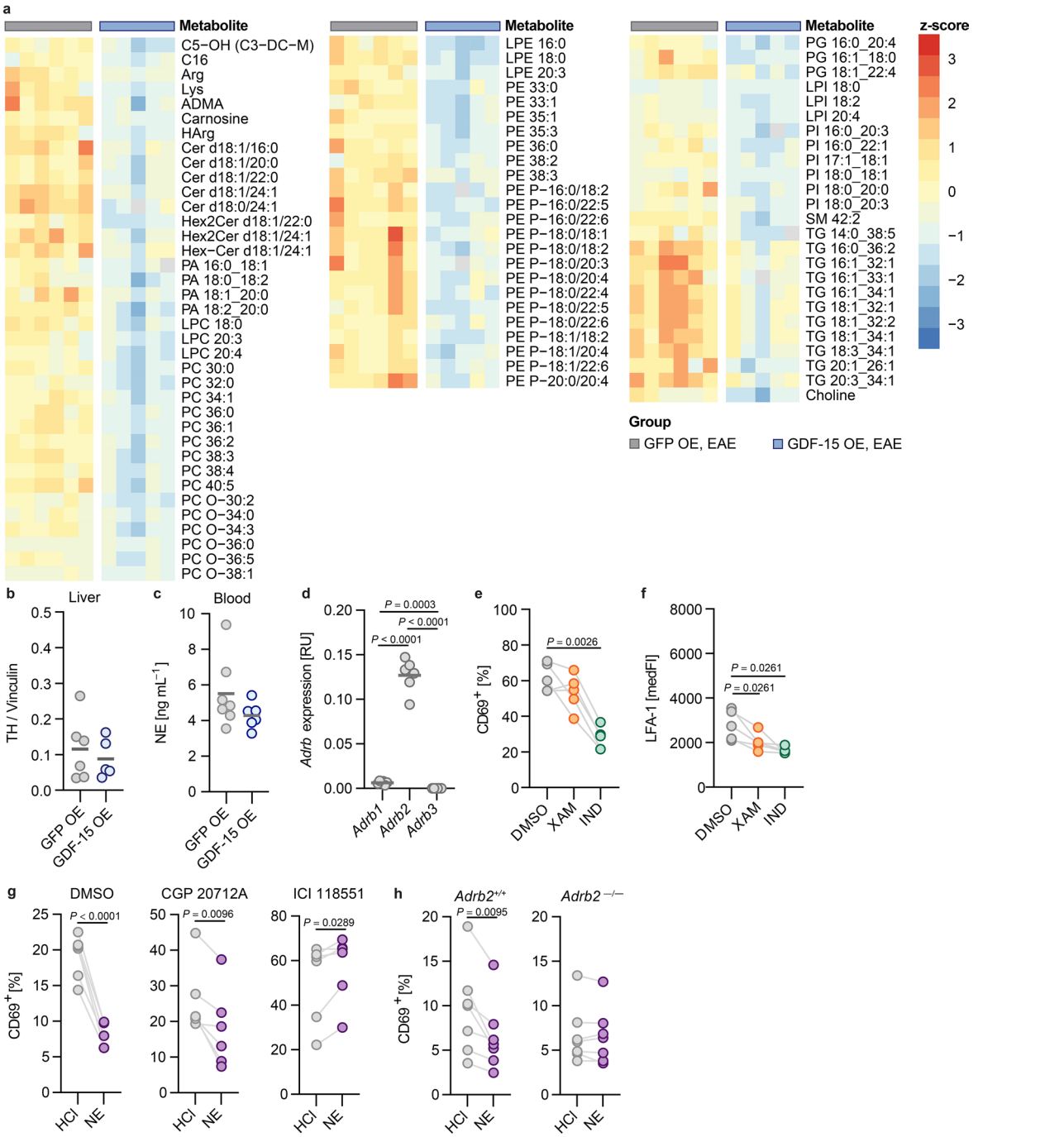

Extended Data Fig. 6 | Selective activation of β2-adrenoceptors inhibits T cell activation. a-c, Female C57BL/6J mice were injected with an rAAV coding for eGFP (GFP OE, $n = 6$) or mouse GDF-15 (GDF-15 OE, $n = 5$). **a**, Metabolomics of plasma collected in the preclinical EAE phase (9 days post immunization, p.i.); $n = 6$ for GFP OE, $n = 5$ for GDF-15 OE. LPC, lysophosphatidylcholine; LPE, lysophosphatidylethanolamine; LPI, lysophosphatidylinositol; PA, phosphatidic acid; PC, phosphatidylcholine; PE, phosphatidylethanolamine; PI, phosphatidylinositol; SM, sphingomyelin; TG, triglyceride. **b**, Quantification of tyrosine hydroxylase (TH) in the liver of rAAV-injected mice by immunoblot. Expression was normalized to vinculin (Vin); $n = 6$ for GFP OE, $n = 5$ for GDF-15 OE. **c**, Blood norepinephrine (NE) concentration in naive female mice with (GFP OE, $n = 7$) or (GDF-15 OE, $n = 6$) three weeks after rAAV injection. **d**, *Adrb1/2/3* expression in $CD4^+$ T cells from female mice measured by RT-qPCR; $n = 6$. **e**, **f**, Primary mouse T cells were stimulated with anti-CD3/CD28 and 10 µM xamoterol (XAM), 10 µM indacaterol (IND) or DMSO; $n = 5$. **e**, Frequency of $CD69^+$ cells and **f**, median fluorescence intensity (medFI) of LFA-1 on total $CD4^+$ T cells stimulated after 24 h. **g**, Primary mouse T cells were stimulated with anti-CD3/CD28 and 10 µM CGP 20712A, 10 µM ICI 118551, or DMSO as vehicle control prior to treatment with 10 µM NE or HCl. Frequency of $CD69^+$ cells within total $CD4^+$ T cells after 24 h; $n = 6$. **h**, Primary T cells from *Adrb2*$^{+/+}$ and *Adrb2*$^{-/-}$ mice were stimulated with anti-CD3/CD28 and 10 µM NE or HCl. Frequency of $CD69^+$ cells within total $CD4^+$ T cells after 24 h; $n = 7$ per group. Individual datapoints represent biological replicates. For (**b**, **c**) an unpaired two-sided Mann-Whitney test was performed. For (**d**-**f**), a paired one-way ANOVA with FDR correction was performed. For (**g**,**h**) paired two-sided *t*-tests were performed. OE, overexpression.

https://doi.org/10.1038/s41590-025-02406-1

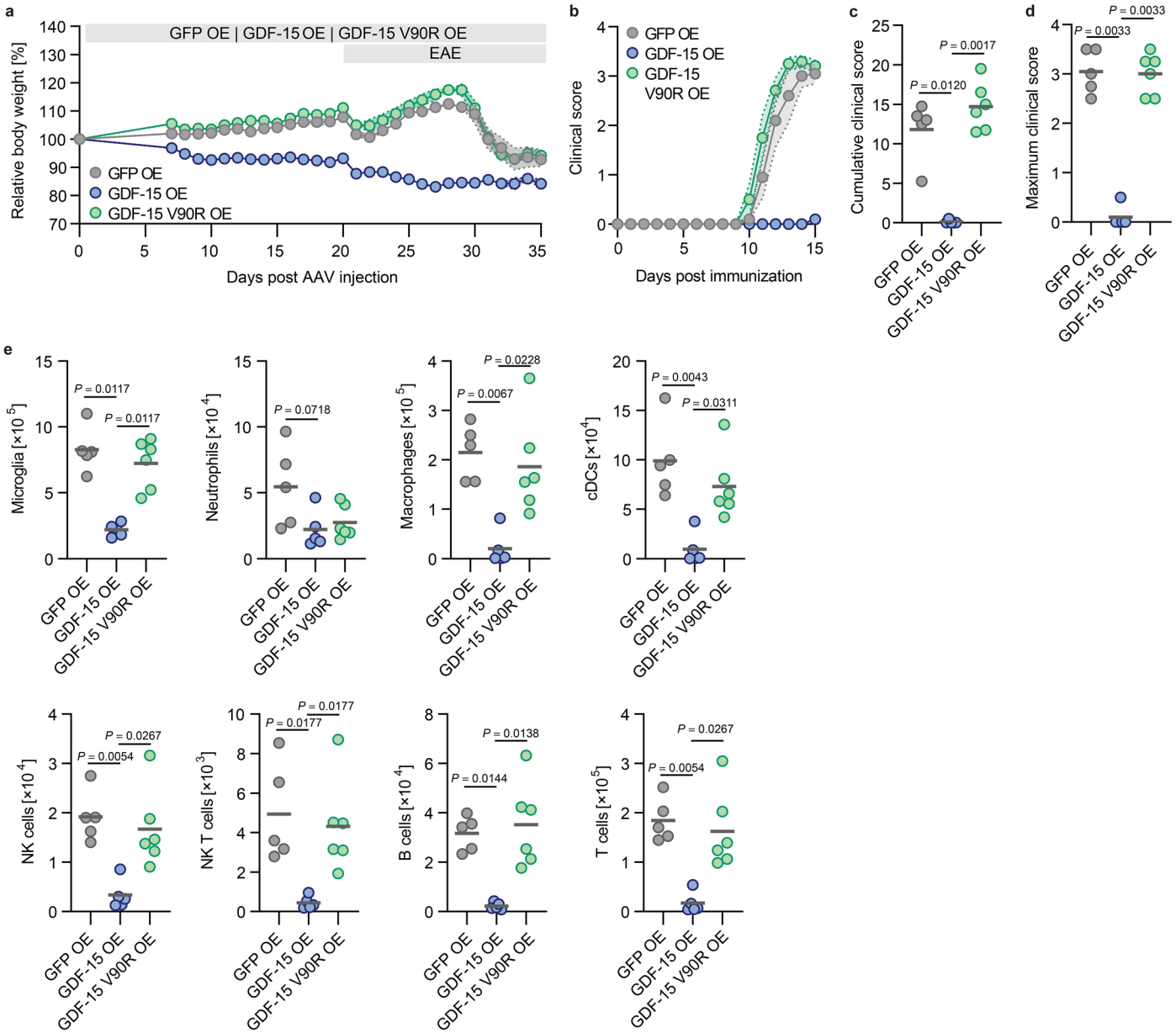

Extended Data Fig. 7 | Loss of GFRAL binding activity abolishes protection of therapeutic GDF-15 delivery. Female C57BL/6J mice were intravenously injected with an rAAV coding for eGFP (GFP OE, $n = 5$), mouse GDF-15 (GDF-15 OE, $n = 5$) or mouse mutant GDF-15 p.Val90Arg (GDF-15 V90R OE, $n = 6$). **a**, Relative body weight change, **b**, mean clinical disease score, **c**, cumulative clinical disease score and **d**, maximum clinical disease score. **e**, Absolute number of microglia and infiltrating immune cells in spinal cord and brain tissue analyzed by flow cytometry on day 15 post immunization. Individual datapoints represent biological replicates. Data are shown as mean ± s.e.m. (**a**, **b**). For (**c**-**e**), a Kruskal-Wallis test with FDR correction was performed. OE, overexpression.

https://doi.org/10.1038/s41590-025-02406-1

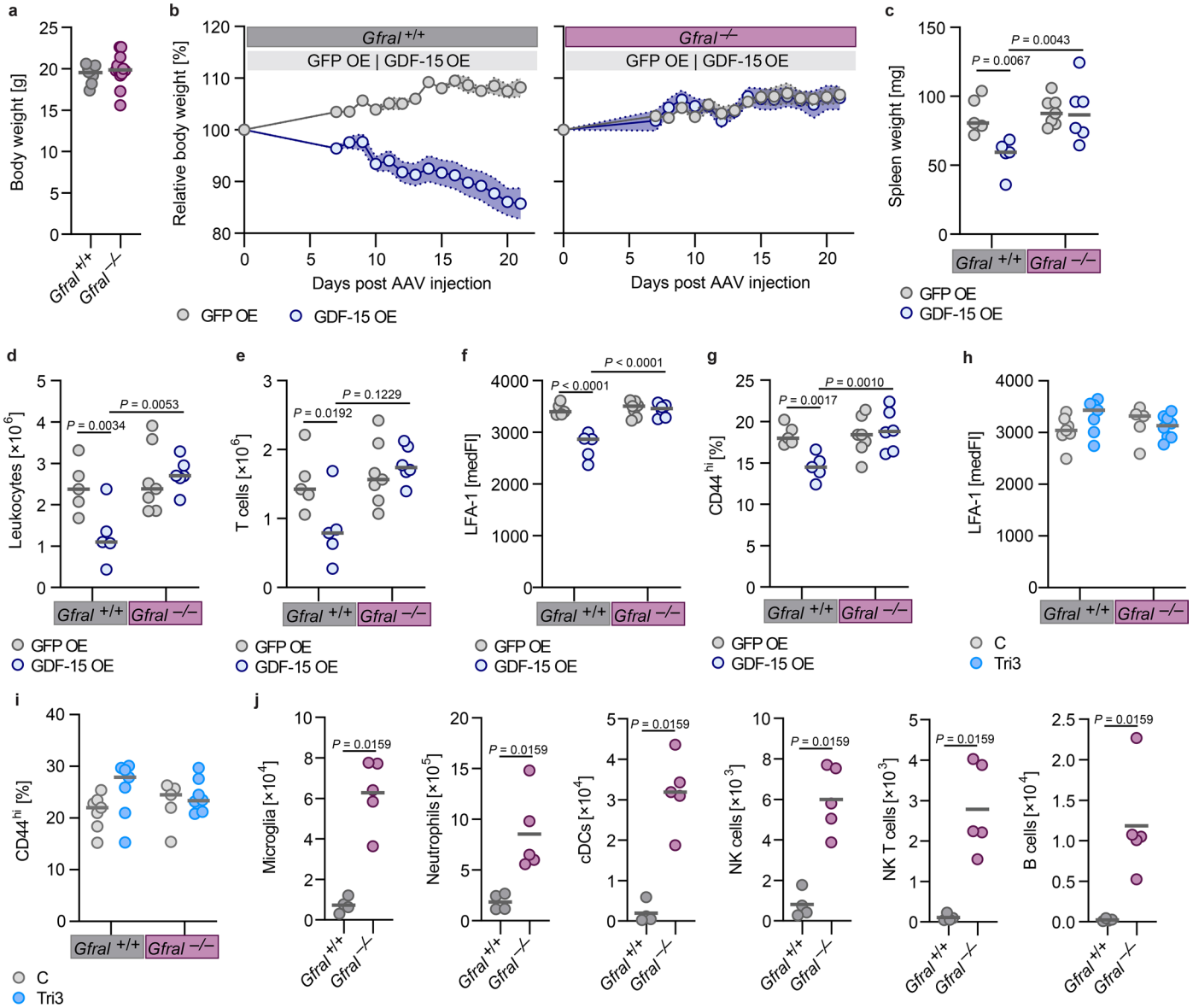

Extended Data Fig. 8 | GDF-15-mediated T cell modulation is GFRAL-dependent. a, Baseline body weight in healthy female *Gfral*$^{-/-}$ ($n = 13$) and *Gfral*$^{+/+}$ ($n = 10$) mice. **b**-**g**, Female mice were injected with an rAAV coding for eGFP (GFP OE) or for mouse GDF-15 (GDF-15 OE); $n = 5$ for *Gfral*$^{+/+}$ GFP OE, $n = 5$ for *Gfral*$^{+/+}$ GDF-15 OE, $n = 7$ for *Gfral*$^{-/-}$ GFP OE, $n = 6$ for *Gfral*$^{-/-}$ GDF-15 OE. **b**, Relative body weight change. **c**, Spleen weight three weeks after rAAV injection. **d**, Absolute number of CD45$^+$ leukocytes in the inguinal lymph nodes (iLNs). **e**, Absolute number of T cells in the iLNs. **f**, Median fluorescence intensity (medFI) of LFA-1 on splenic CD8$^+$ T cells. **g**, Frequency of CD44^{hi} CD8$^+$ T cells in the spleen. **h**-**i**, Semi-allogeneic pregnancy was induced in *Gfral*$^{+/+}$ and *Gfral*$^{-/-}$ mice. The expression of selected markers on splenic CD4$^+$ T cells was analyzed in trimester 3 (Tri3; $n = 7$ for *Gfral*$^{+/+}$ and $n = 8$ for *Gfral*$^{-/-}$) animals or non-pregnant littermate controls (C; $n = 7$ for *Gfral*$^{+/+}$ and $n = 5$ for *Gfral*$^{-/-}$). **h**, MedFI of LFA-1, **i**, frequency of CD44^{hi} cells. **j**, Female *Gfral*$^{+/+}$ ($n = 4$) and *Gfral*$^{-/-}$ ($n = 5$) mice were injected with an GDF-15 OE rAAV and EAE was induced three weeks later. Quantification of infiltrating immune cells in spinal cord and brain tissue on day 15 post immunization. Individual datapoints represent biological replicates. Data are shown as mean ± s.e.m. (**b**). In (**a**, **j**) two-sided Mann-Whitney tests were performed. In (**c**-**i**) two-way ANOVA with FDR correction was used. OE, overexpression.

https://doi.org/10.1038/s41590-025-02406-1

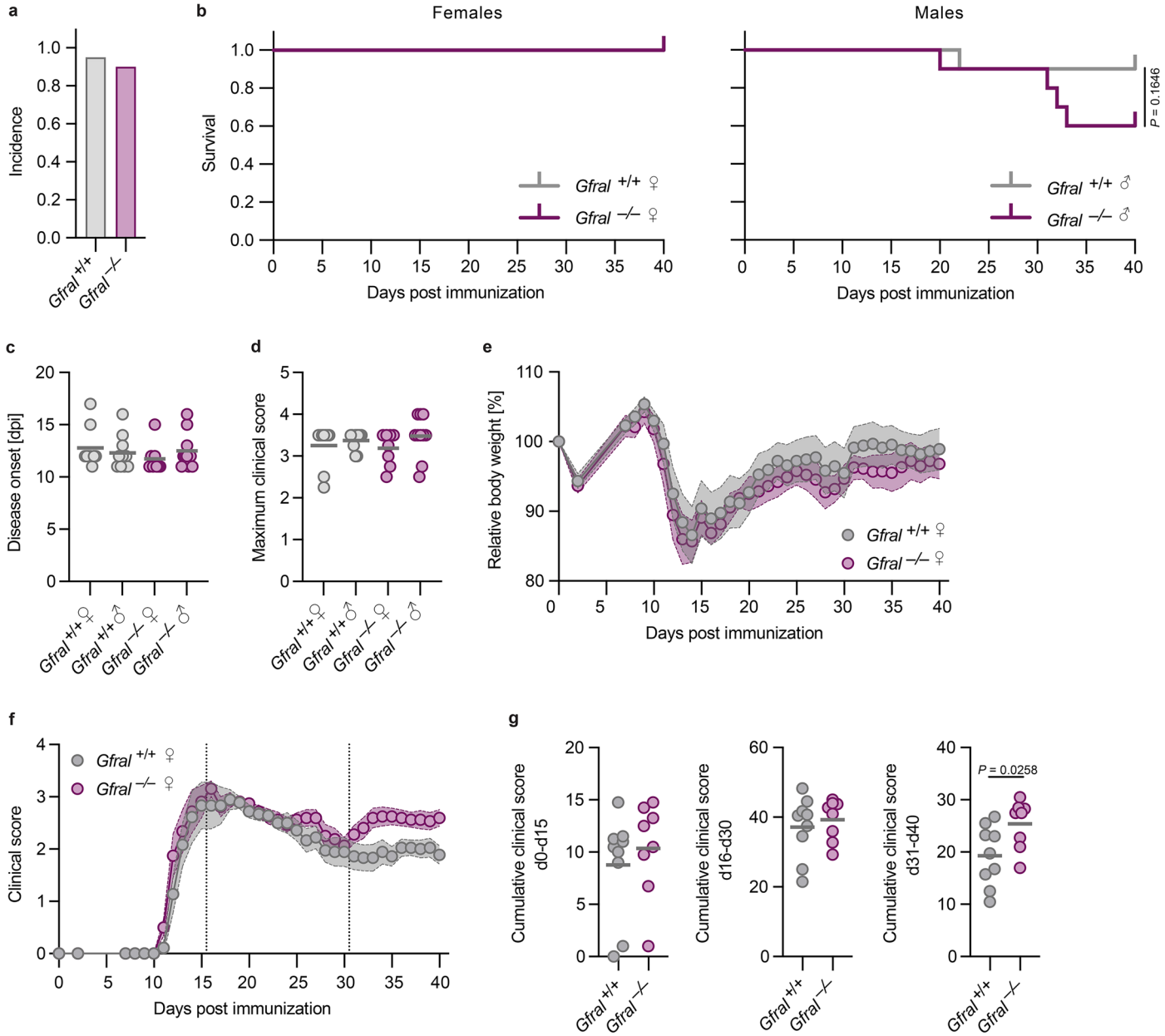

Extended Data Fig. 9 | *Gfral* deficiency exacerbates neuroinflammation. EAE was induced in *Gfral*-proficient ($Gfral^{+/+}$, $n = 20$) and -deficient ($Gfral^{-/-}$, $n = 20$) mice. **a**, Incidence, **b**, survival, **c**, disease onset, and **d**, maximum clinical score in female ($Gfral^{+/+}$, $n = 9$; $Gfral^{-/-}$, $n = 8$) and male ($Gfral^{+/+}$, $n = 10$; $Gfral^{-/-}$, $n = 10$) littermates. **e**, Relative body weight loss and **f**, mean clinical disease score in female mice ($Gfral^{+/+}$, $n = 9$; $Gfral^{-/-}$, $n = 8$). **g**, Cumulative clinical score until acute phase (d0-d15), remission phase (d16-30) and relapse phase (d31-40) in female mice ($Gfral^{+/+}$, $n = 9$; $Gfral^{-/-}$, $n = 8$). Individual datapoints represent biological replicates. Data are shown as mean ± s.e.m. (**e**, **f**). For (**a**), a Fisher's exact test was used. In (**b**) a Wilcoxon test was performed. For (**c**, **d**), a Kruskal-Wallis test with FDR correction was performed. In (**g**) a two-sided Mann-Whitney tests were performed. OE, overexpression.

https://doi.org/10.1038/s41590-025-02406-1

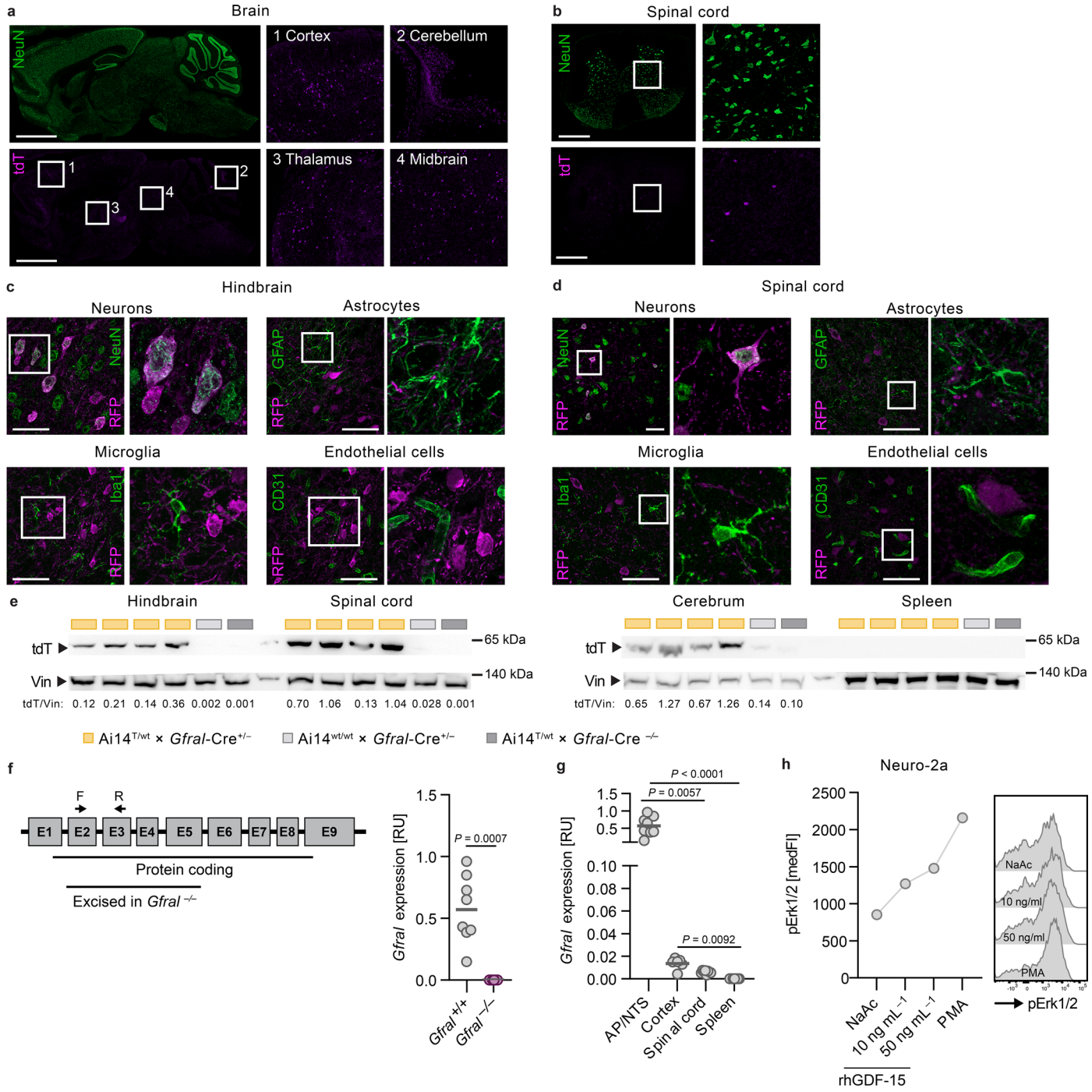

Extended Data Fig. 10 | *Gfral* expression is limited to the CNS. a, Sagittal brain section of GFRAL-Cre × Ai14 reporter mice showing endogenous tdTomato (tdT) signal. Scale bar indicates 2 mm. **b**, Cervical spinal cord section of GFRAL-Cre × Ai14 reporter mice showing endogenous tdT. Scale bars, 500 µm. **c**, Z-stacks in hindbrain sections showing GFRAL-tdT$^+$ cells counterstained with anti-RFP and for markers of neurons (NeuN$^+$), astrocytes (GFAP$^+$), microglia (Iba1$^+$), and endothelial cells (CD31$^+$). Scale bars, 50 µm. **d**, Z-stacks in cervical spinal cord sections showing GFRAL-tdT$^+$ cells counterstained with anti-RFP and for markers of neurons, astrocytes, microglia, and endothelial cells. Scale bars, 50 µm. **e**, Immunoblot for RFP/tdTomato in tissue lysates from hindbrain, spinal cord, cerebrum, and spleen. $n = 4$ for experimental group Ai14$^{T/wt}$ x *Gfral*-Cre$^{+/-}$; $n = 1$ for each control. **f**, Scheme for oligonucleotide design targeting the mouse *Gfral* locus for RT-qPCR and validation of selected oligonucleotide pair in area postrema (AP)/nucleus tractus solitarius (NTS) tissue from *Gfral*$^{+/+}$ ($n = 8$) and *Gfral*$^{-/-}$ mice ($n = 6$). **g**, *Gfral* expression in healthy female and male C57BL/6J mice measured in AP/NTS ($n = 8$), cortex ($n = 6$), spinal cord ($n = 8$), and spleen ($n = 7$) by RT-qPCR. **h**, Neuro-2a cells were stimulated with increasing doses of recombinant human GDF-15 (rhGDF-15), 100 ng mL^{-1} PMA or NaAc for 30 minutes. Median fluorescence intensity (medFI) of pErk1/2 was determined by flow cytometry. Individual datapoints represent biological replicates. In (**a**-**d**) images from one representative animal are shown. In (**h**) data from one representative experiment is shown. For (**f**) a two-sided Mann-Whitney test was performed. In (**g**) a Kruskal-Wallis test with FDR correction was used.

nature portfolio

Corresponding author(s): Manuel Friese

Last updated by author(s): Nov 18, 2025

Reporting Summary

Nature Portfolio wishes to improve the reproducibility of the work that we publish. This form provides structure for consistency and transparency in reporting. For further information on Nature Portfolio policies, see our Editorial Policies and the Editorial Policy Checklist.

Statistics

For all statistical analyses, confirm that the following items are present in the figure legend, table legend, main text, or Methods section.

n/a	Confirmed	
☐	☒	The exact sample size (*n*) for each experimental group/condition, given as a discrete number and unit of measurement
☐	☒	A statement on whether measurements were taken from distinct samples or whether the same sample was measured repeatedly
☐	☒	The statistical test(s) used AND whether they are one- or two-sided *Only common tests should be described solely by name; describe more complex techniques in the Methods section.*
☒	☐	A description of all covariates tested
☐	☒	A description of any assumptions or corrections, such as tests of normality and adjustment for multiple comparisons
☐	☒	A full description of the statistical parameters including central tendency (e.g. means) or other basic estimates (e.g. regression coefficient) AND variation (e.g. standard deviation) or associated estimates of uncertainty (e.g. confidence intervals)
☐	☒	For null hypothesis testing, the test statistic (e.g. *F*, *t*, *r*) with confidence intervals, effect sizes, degrees of freedom and *P* value noted *Give P values as exact values whenever suitable.*
☒	☐	For Bayesian analysis, information on the choice of priors and Markov chain Monte Carlo settings
☒	☐	For hierarchical and complex designs, identification of the appropriate level for tests and full reporting of outcomes
☒	☐	Estimates of effect sizes (e.g. Cohen's *d*, Pearson's *r*), indicating how they were calculated

Our web collection on statistics for biologists contains articles on many of the points above.

Software and code

Policy information about availability of computer code

Data collection	Flow cytometric nuclei or cell sorting: BD FACSDiva v9.0.1 software (BD Bioscience) to run BD FACS Aria III. Flow cytometry data collection: FACSDiva software version 9.1 software (BD Biosciences) to run BD Symphony A3. Bulk RNAsequencing: NovaSeq6 000 platform (Illumina). Confocal imaging: Zeiss LSM 900 Airyscan 2 confocal microscope equipped with ZEN blue software v3.9. Immunoblots: LAS4000 Image-Reader software. RT-qPCR: QuantStudio Flex 6 Real-Time PCR System. Metabolomics: WebIDQ cloud-based software package (BIOCRATES, version 2024).
Data analysis	Image analysis fluorescence microscopy and immunoblots: ImageJ 1.54i Flow cytometry: FlowJo version 10.9 (BD Biosciences) Bulk RNAsequencing: STAR v2.7.9a, featureCounts v1.5.1, DESeq2 v1.40.2, biomaRt v2.56.1, ggplot2 v3.4.3. Data representation and statistics: Prism 10.4.2 (GraphPad). Metabolomics: WebIDQ cloud-based software package (BIOCRATES, version 2024). Power analysis: G*Power 3.1 RT-qPCR: Thermo Fisher Cloud

For manuscripts utilizing custom algorithms or software that are central to the research but not yet described in published literature, software must be made available to editors and reviewers. We strongly encourage code deposition in a community repository (e.g. GitHub). See the Nature Portfolio guidelines for submitting code & software for further information.

Data

Policy information about availability of data

All manuscripts must include a data availability statement. This statement should provide the following information, where applicable:

- Accession codes, unique identifiers, or web links for publicly available datasets
- A description of any restrictions on data availability
- For clinical datasets or third party data, please ensure that the statement adheres to our policy

Sequencing data generated for this study are available through the Gene Expression Omnibus under accession number GSE288193. All other data are available in the main text or the supplementary materials.

Research involving human participants, their data, or biological material

Policy information about studies with human participants or human data. See also policy information about sex, gender (identity/presentation), and sexual orientation and race, ethnicity and racism.

Reporting on sex and gender	We report the sex of all participants in Supplementary Table 1 to 4.
Reporting on race, ethnicity, or other socially relevant groupings	For this study, we selected participants blind to their age and ethnicity. Most participants were female since we study the dynamics of GDF-15 in pregnancy. The demographic characteristics are described in Supplementary Table 1 to 4.
Population characteristics	For this study, we selected participants blind to their age ethnicity based on the availability of frozen serum samples. The demographic characteristics are described in Supplementary Table 1 to 4.
Recruitment	MS patients and healthy individuals were recruited through the MS outpatient clinic of the Department of Neurology, University Medical Center Hamburg-Eppendorf. Pregnant women were recruited through the PRINCE (PRenatal IdeNtification of Children's HEalth) study which enrolled women of legal age experiencing a singleton pregnancy during their first trimester (gestational weeks 12–14). Serum samples of pregnant women who experienced miscarriage or performed elective abortion were collected during routine blood sampling and processed according to standard laboratory methods at the Laboratory for Pediatric Rheumatology/Special Immunology at the University Hospital Wuerzburg. Participants did not receive any financial compensation.
Ethics oversight	MS patients and healthy individuals: Hamburg Chamber of Commerce Act for the Health Professions, registration number PV4405. Pregnant women recruited through the PRINCE: Hamburg Chamber of Physicians (license number PV3694). Pregnant women who experienced miscarriage or performed elective abortion: ethics protocol numbers 28/08 and 239/10. The study adhered to the principles outlined in the Declaration of Helsinki for medical research involving human subjects.

Note that full information on the approval of the study protocol must also be provided in the manuscript.

Field-specific reporting

Please select the one below that is the best fit for your research. If you are not sure, read the appropriate sections before making your selection.

☒ Life sciences ☐ Behavioural & social sciences ☐ Ecological, evolutionary & environmental sciences

For a reference copy of the document with all sections, see nature.com/documents/nr-reporting-summary-flat.pdf

Life sciences study design

All studies must disclose on these points even when the disclosure is negative.

Sample size	Sample sizes were estimated based on previous extensive experience in the laboratory with the EAE model. For in vitro experiments with primary cells at least 4 biological replicates were used based on 3R principles, sample sizes of previous published studies and the fact that experiments were performed in inbred mice.
Data exclusions	In the EAE model, mice without ulcerations at the injection site prior to disease onset were excluded from the analyses. For immunohistochemical analysis specimens with impaired tissue integrity were removed from the analysis. No samples were excluded from the analysis based on outlier detection. For the TH immunoblot in DREADD animals the last specimen was excluded from analysis due to incomplete transfer to the membrane.
Replication	EAE experiments were performed twice (Gdf15-/-) with different readouts or repeated multiple times with adapted strategies (GDF-15 OE, combined i.e. with paired feeding or mutant GDF-15). All attempts to replicate findings were successful. Experiments with Gfral-/- and DREADD animals were only performed once, but with sufficient power to detect differences. All data derived from primary cells/tissues were performed with biological replicates. Experiments with T cells treated with ADRB agonists and antagonists were performed at least twice with similar results.

For experiments with cell lines at least three independent experiments were performed with similar results, unless stated otherwise.

Randomization

In EAE experiments, mice were randomly assigned to treatment or control groups (Control vs effector AAV, treatment vs vehicle). These mice were mixed within cages to minimize cage-specific effects. Only for paired-feeding experiments animals belonging to the same group were housed together in groups of 2-3 animals per cage since food intake had to monitored for each group separetely. For experiments with transgenic mice (Gdf15-/-, Gfral-/-, DREADD) cages contained littermates of different genotypes to minimize cage-effects.

Blinding

Mouse scoring was conducted in a blinded manner, with researchers not aware of genotype, the injected AAV or the treatment to prevent observer bias. Since for the paired-feeding experiments animals belonging to different experimental groups had to be housed separately (see randomization), one researcher monitored food consumption, while a second independent researcher assessed the clinical score. For all downstream analyses (histology, flow cytometry, etc.) the reseacher was blinded during acquisition and analysis. The analysis of plasma or serum samples was performed in a blinded manner as the researcher measuring GDF-15 or catecholamines was not aware of the group assignment.

Reporting for specific materials, systems and methods

We require information from authors about some types of materials, experimental systems and methods used in many studies. Here, indicate whether each material, system or method listed is relevant to your study. If you are not sure if a list item applies to your research, read the appropriate section before selecting a response.

Materials & experimental systems

n/a	Involved in the study
☐	☒ Antibodies
☐	☒ Eukaryotic cell lines
☒	☐ Palaeontology and archaeology
☐	☒ Animals and other organisms
☒	☐ Clinical data
☒	☐ Dual use research of concern
☒	☐ Plants

Methods

n/a	Involved in the study
☒	☐ ChIP-seq
☐	☒ Flow cytometry
☒	☐ MRI-based neuroimaging

Antibodies

Antibodies used

ACSA-2 APC Miltenyi Biotec 130-117-535 Rat IH3-18A3 1:50 IF, IHC, FC
BTLA PE BioLegend 139107 Armenian Hamster 6A6 1:100 FC - Quality tested
CD3 BioLegend 100301 Armenian Hamster 145-2C11 1:200 FC - Quality tested
CD4 Pacific Blue BioLegend 100531 Rat RM4-5 1:400 FC - Quality tested
CD4 BUV395 BD Bioscience 563790 Rat GK1.5 1:200 FC (Routinely Tested)
CD4 BV711 BioLegend 100447 Rat GK1.5 1:200 FC - Quality tested
CD8α BV785 BioLegend 100750 Rat 53-6.7 1:200 FC - Quality tested
CD8α Pacific Blue BioLegend 100725 Rat 53-6.7 1:400 FC - Quality tested
CD11b BUV395 BD Bioscience 563553 Rat M1/70 1:400 FC (Routinely Tested)
CD11b BV785 BioLegend 101243 Rat M1/70 1:200 FC - Quality tested
CD11c PE-Cy7 BioLegend 117318 Rat N418 1:400 FC - Quality tested
CD19 BUV661 BD Bioscience 612971 Rat 1D3 1:400 FC (Routinely Tested)
CD19 BUV805 BD Bioscience 568287 Rat 1D3 1:400 FC (Routinely Tested)
CD19 PE-Cy7 BioLegend 115519 Rat 6D5 1:400 FC - Quality tested
CD25 PE BioLegend 102008 Rat PC61 1:100 FC - Quality tested
CD29 PE-Cy7 BioLegend 102222 Armenian Hamster HMβ1-1 1:100 FC - Quality tested
CD31 R&D systems AF3628 Goat polyclonal 1:100 ELISA, WB, ICH, ICC, FC
CD44 APC-Cy7 BioLegend 103028 Rat IM7 1:200 FC - Quality tested
CD44 PerCP-Cy5.5 BioLegend 103032 Rat IM7 1:200 FC - Quality tested
CD45 BioLegend 103101 Rat 30-F11 1:200 FC - Quality tested
CD45 APC-Cy7 BioLegend 103116 Rat 30-F11 1:200 FC - Quality tested
CD45 FITC BioLegend 103108 Rat 30-F11 1:200 FC - Quality tested
CD45 Pacific Blue BioLegend 103126 Rat 30-F11 1:200 FC - Quality tested
CD49d PE BioLegend 103607 Rat R1-2 1:50 FC - Quality tested
CD68 BioLegend 137002 Rat FA-11 1:1000 FC - Quality tested
CD69 PE-Cy7 BioLegend 104512 Armenian Hamster H1.2F3 1:200 FC - Quality tested
CD127 BV785 BioLegend 135037 Rat A7R34 1:100 FC - Quality tested
CX3CR1 Pacific Blue BioLegend 149038 Mouse SA011F11 1:200 FC - Quality tested
F4/80 BV421 BioLegend 123132 Rat BM8 1:100 FC - Quality tested
GDF-15 Evitria custom-made Mouse 297 20 µg/ml N/A
GFAP Merck Millipore AB5541 Chicken polyclonal 1:800 1:800 ICC, IHC, WB
GFP Abcam ab13970 Chicken polyclonal 1:2000 WB, ICC/IF
GPNMB eFluor660 Invitrogen 50-5708-80 Rat CTSREVL 1:50 FC
HA Sigma-Aldrich 11867423001 Rat 3F10 1:400 ELISA, IHC, IP, WB
I-A/I-E BUV805 BD Bioscience 748844 Rat M5/114.15.2 1:200 FC (Routinely Tested)
Iba1 Synaptic Systems 234308 Guinea Pig Gp311H9 1:500 WB, IP, ICC, IHC

Iba1 Wako 019-19741 Rabbit polyclonal 1:1000 ICC, IHC
LFA-1 APC BioLegend 141010 Rat H155-78 1:100 FC - Quality tested
Ki-67 eFluor 660 eBioscience 50-5698-80 Rat SolA15 1:50 IHC, ICC, FC
Ly6C PE BioLegend 128008 Rat HK1.4 1:200 FC - Quality tested
Ly6G PerCP-Cy5.5 BioLegend 127616 Rat 1A8 1:100 FC - Quality tested
NeuN Millipore ABN91 Chicken polyclonal 1:400 WB, ICC, IHC
NeuN Synaptic Systems 266004 Guinea Pig polyclonal 1:250 1:250 ICC, IHC
NeuN Alexa Fluor 647 Abcam ab190565 Rabbit EPR12763 1:500 IHC, ICC
Nk1.1 APC BioLegend 108710 Mouse PK136 1:100 FC - Quality tested
NK1.1 PE Invitrogen 12-5941-82 Mouse PK136 1:200 FC
NK1.1 PE-Cy7 BioLegend 108714 Mouse PK136 1:200 FC - Quality tested
Nur77 AF488 Invitrogen 53-5965-82 Mouse 12.14 1:50 FC
P2RY12 PE BioLegend 848004 Rat S16007D 1:100 FC - Quality tested
PD-1 (CD279) BV421 BioLegend 109121 Rat RMP1-30 1:100 FC - Quality tested
pErk1/2 BioLegend 369516 Mouse 6B8B69 1:20 ICFC - Quality tested
RFP ChromoTek 5f8 Rat 5F8 1:1000 IF, ELISA
RFP Rockland R10367 Rabbit polyclonal 1:1000 ELISA, IF, IHC, WB
Tubulin-β3 BioLegend 801213 Mouse TUJ1 1:200 IHC-P, WB, ICC
TCRβ BUV737 BD Bioscience 612821 Armenian Hamster H57-597 1:100 FC (Routinely Tested)
TCRβ BV421 BioLegend 109230 Armenian Hamster H57-597 1:200 FC - Quality tested
Tyrosine hydroxylase Proteintech 25859-1-AP Rabbit polyclonal 1:5000 WB, IP, IHC, IF
Tyrosine hydroxylase Sigma-Aldrich AB152 Rabbit polyclonal 1:500 ELISA, IF, IHC, IP, WB
Vinculin Merck V9131 Mouse hVin-1 1:1000 WB, IF, IHC

Donkey Ig chicken Alexa Fluor 488 Jackson Immuno 703-545-155 Donkey polyclonal 1:500 ICC, IHC
Donkey Ig chicken Alexa Fluor Cy3 Jackson Immuno 703-165-155 Donkey polyclonal 1:500 ICC, IHC
Donkey Ig chicken Alexa Fluor 647 Jackson Immuno 703-606-155 Donkey polyclonal 1:500 ICC, IHC
Donkey Ig goat Alexa Fluor 488 Abcam ab150129 Donkey polyclonal 1:500 ELISA, IHC-Fr, IHC-P, FC, ICC/IF
Donkey Ig goat Alexa Fluor 555 Abcam ab150130 Donkey polyclonal 1:500 ELISA, IHC-Fr, IHC-P, FC, ICC/IF
Donkey Ig guinea pig Alexa Fluor 488 Jackson Immuno 706-545-148 Donkey polyclonal 1:500 ICC, IHC
Donkey Ig guinea pig Alexa Fluor Cy3 Jackson Immuno 706-165-148 Donkey polyclonal 1:500 ICC, IHC
Donkey Ig guinea pig Alexa Fluor 647 Jackson Immuno 706-605-148 Donkey polyclonal 1:500 ICC, IHC
Donkey Ig rabbit Alexa Fluor 488 Abcam ab150073 Donkey polyclonal 1:500 ELISA, IHC-Fr, IHC-P, FC, ICC/IF
Donkey Ig rabbit Alexa Fluor 555 Abcam ab150062 Donkey polyclonal 1:500 ELISA, IHC-Fr, IHC-P, FC, ICC/IF
Donkey Ig rat Alexa Fluor 555 Abcam ab150150 Donkey polyclonal 1:500 ELISA, IHC-Fr, IHC-P, FC, ICC/IF
Donkey Ig rabbit Alexa Fluor 647 Abcam ab181347 Donkey polyclonal 1:500 ELISA, IHC-Fr, IHC-P, FC, ICC/IF
Donkey Ig rat Alexa Fluor 647 Abcam ab150151 Donkey polyclonal 1:500 ELISA, IHC-Fr, IHC-P, FC, ICC/IF
Donkey Ig Mouse Alexa Fluor 647 Abcam ab150111 Donkey polyclonal 1:500 ELISA, IHC-Fr, IHC-P, FC, ICC/IF
DyLight 649 IgG Armenian hamster BioLegend 405505 Goat polyclonal 1:200 FC - Quality tested

Goat anti-mouse HRP LICORbio 926-80010 Goat polyclonal 1:10000 WB
Goat anti-rabbit HRP Cell Signaling 7074 Goat polyclonal 1:5000 WB, IHC, ELISA
Goat anti-rat HRP Cell Signaling 7077 Goat polyclonal 1:5000 WB, IHC, ELISA

Validation

Antibody validation for the species is provided for all commercially available antibodies on the relevant manufacturer's website accessible via the catalogue numbers which are provided above.

Eukaryotic cell lines

Policy information about cell lines and Sex and Gender in Research

Cell line source(s)

HEK 293T (ACC 635, DMSZ, purchased in 2017), Neuro-2a (ACC 148, DSMZ, purchased 2022), SIM-A9 (T0247-GVO-ABM, Biocat, purchased 2024).

Authentication

All cell lines used in this study were purchased from authorized vendors.

Mycoplasma contamination

All cell lines were regularly checked for mycoplasma contamination using the VenorGeM Advance kit (Minerva biolabs, 11-7024) according to the manufacturer's instructions. Cell lines were free of mycoplasma contamination.

Commonly misidentified lines
(See ICLAC register)

None of the cell lines used in this study is listed in the registry.

Animals and other research organisms

Policy information about studies involving animals; ARRIVE guidelines recommended for reporting animal research, and Sex and Gender in Research

Laboratory animals

All mice (C57BL/6J and BALB/c wild-type purchased from Charles River; Gdf15–/–; Gfral–/–, Gfral-Cre (purchased from the Jackson Laboratory, #036750), Ai14, LSL-hM3Dq-DREADD, Gfral-Cre × Ai14, Gfral-Cre × LSL-hM3Dq-DREADD, Adrb2–/– were kept under specific pathogen-free conditions in the central animal facility of the University Medical Center Hamburg-Eppendorf. Adult mice (6–20 weeks old) from both sexes were used, unless otherwise stated; mice were sex- and age-matched in all experiments. The mice were kept in a 12-hour light/dark diurnal cycle, 22 ± 2 °C, 40-60 % humidity and given ad libitum access to standard chow (Altromin, 1328P) and water, unless otherwise stated. EAE mice additionally received DietGel® Recovery (Ssniff; H007-72065).
We thank Jens Strelau (Department of Functional Neuroanatomy, University of Heidelberg, Heidelberg, Germany) for providing

Gdf15–/– animals, Christine Gee Gee (Institute for Synaptic Neuroscience, ZMNH, University Medical Center Hamburg-Eppendorf, Hamburg, Germany) for providing LSL-hM3Dq-DREADD animals, Ora Ohana for providing Ai14 animals (Institute for Molecular and Cellular Cognition, ZMNH, University Medical Center Hamburg-Eppendorf, Hamburg, Germany) to generate GFRAL reporter animals, and Johannes Keller and Anke Baranowsky (Department of Trauma and Orthopaedic Surgery, University Medical Center Hamburg-Eppendorf, Hamburg, Germany) for providing Adrb2–/– animals.

Wild animals: This study does not involve wild animals.

Reporting on sex: For EAE experiments involving C57BL/6J WT mice, only female animals were included. For all other experiments the sex is specified in the figure legend.

Field-collected samples: This study does not include field-collected samples.

Ethics oversight: All animal care and experimental procedures were conducted in accordance with institutional guidelines and met the requirements of the German legal authorities. Ethical approvals were obtained from the State Authority of Hamburg, Germany (Behörde für Justiz und Verbraucherschutz, Freie und Hansestadt Hamburg; approval no. 45/17, N007/22, N108/24).

Note that full information on the approval of the study protocol must also be provided in the manuscript.

Plants

Seed stocks: No plants were uses in this study

Novel plant genotypes: *Describe the methods by which all novel plant genotypes were produced. This includes those generated by transgenic approaches, gene editing, chemical/radiation-based mutagenesis and hybridization. For transgenic lines, describe the transformation method, the number of independent lines analyzed and the generation upon which experiments were performed. For gene-edited lines, describe the editor used, the endogenous sequence targeted for editing, the targeting guide RNA sequence (if applicable) and how the editor was applied.*

Authentication: *Describe any authentication procedures for each seed stock used or novel genotype generated. Describe any experiments used to assess the effect of a mutation and, where applicable, how potential secondary effects (e.g. second site T-DNA insertions, mosiacism, off-target gene editing) were examined.*

Flow Cytometry

Plots

Confirm that:

☒ The axis labels state the marker and fluorochrome used (e.g. CD4-FITC).

☒ The axis scales are clearly visible. Include numbers along axes only for bottom left plot of group (a 'group' is an analysis of identical markers).

☒ All plots are contour plots with outliers or pseudocolor plots.

☒ A numerical value for number of cells or percentage (with statistics) is provided.

Methodology

Sample preparation:

Flow cytometric nucleus sorting:
Nuclei of mouse spinal cords were isolated with the Nuclei Isolation Kit (Sigma-Aldrich, NUC101) according to the manufacturer's protocol with minor modifications. Briefly, mice were sacrificed with CO2 and perfused with cold PBS. Whole spinal cords were removed and stored at –80 °C. The tissue was mechanically dissociated with a scalpel on a petri dish placed on a cooled metal block. Tissue was added to 2 mL of EZ buffer (Sigma-Aldrich, NUC101) and further dissociated using a glass douncer (Sigma-Aldrich, D9063). After 5 minutes incubation on ice, the homogenate was centrifuged (500 × g, 5 minutes, 4 °C) and the pellet was washed in 2 mL of EZ buffer, followed by two washing steps in nuclei incubation buffer (340 mM sucrose, 2 mM MgCl2, 25 mM KCl, 65 mM glycerophosphate, 5% glycerol, 1 mM EDTA, 1% bovine serum albumin). Nuclei were filtered using a 30 µm filter and directly stained with AF647-labeled NeuN antibody and 0.25 µg mL–1 propidium iodide (BioLegend, 421301). NeuN+ and NeuN– nuclei were sorted using a BD FACSAria III cell sorter (BD Biosciences) with a 70 µm nozzle.

Flow cytometric cell sorting:
For isolation of astrocytes and immune cells from spinal cord tissue, we incorporated the transcriptional inhibitor actinomycin D (ActD) throughout the workflow. Spinal cord tissue from EAE animals and healthy controls was collected in RPMI-1640 medium (PAN Biotech, P04-18500) supplemented with 25 mM HEPES (Gibco, 15630056) and 30 µM ActD (Cell Signaling, 15021S) after transcardial PBS perfusion. Tissue was dissociated into single-cell suspensions in 1 mg mL–1 collagenase A (Roche, 11088793001) and 200 IU mL–1 DNase I (Merck Millipore, 260913) using the gentleMACS Octo Dissociator (Miltenyi Biotec, program: Multi_F). The dissociated tissue was applied to a 70 µm cell strainer, and the filter was rinsed three times with RPMI-1640 supplemented with 25 mM HEPES and 3 µM ActD. Dissociated tissue was collected after centrifugation at 500 × g for 5 minutes, 4 °C and immune and glia cells were enriched using a discontinuous density gradient with Percoll PLUS (GE Healthcare, 17-5445-01). Isotonic Percoll solutions were prepared with HBSS and supplemented with 3 µM ActD. After centrifugation at 1350 × g, 4° C for 30 minutes, cells were collected from the interphase between the 30% Percoll and 70% Percoll layer. Cells were washed in FACS buffer (PBS, 1 mM EDTA, 1% BSA (Miltenyi Biotec, 130-091-376), 10

mM HEPES) at 650 × g, 4° C for 10 minutes. Nonspecific Fc receptor–mediated antibody binding was blocked by pre-incubation with TruStain FcX anti-mouse CD16/32 antibody (BioLegend, 101320) for 10 minutes at 4 °C before staining with surface antibodies in FACS buffer for 20 minutes at 4 °C. All antibodies used in this study are listed in Extended Data Table 7. Cells were washed and resuspended in FACS buffer supplemented with 0.4 U µL–1 RiboLock RNase Inhibitor (Thermo Fisher Scientific, EO0382) and 2.5 µM Helix NP Green (BioLegend, 425303) to exclude dead cells.

Immune cell isolation for flow cytometry:
Inguinal lymph nodes and spleen samples were homogenized through a 70 µm cell strainer and washed with PBS (500 × g, 5 minutes, 4 °C). Red blood cells were lysed as described above. Brain and spinal cord tissue were collected after transcardial PBS perfusion and dissociated into single cell suspensions in 1 mg mL–1 collagenase A and 0.1 mg mL–1 DNase I using the gentleMACS Octo Dissociator (program: Multi_F). The dissociated tissue was applied to a 70 µm cell strainer, and immune and glia cells were enriched using a discontinuous density gradient (GE Healthcare, GE17-0891-01). Cells were collected from the interphase as described above. Nonspecific Fc receptor–mediated antibody binding was blocked by pre-incubation with TruStain FcX anti-mouse CD16/32 antibody prior to staining of surface antibodies in Brilliant Stain Buffer (BD Biosciences) for 30 minutes at 4 °C. For staining of intranuclear proteins cells were fixed in 1X Fixation/Permeabilization working solution for 45 minutes at 4 °C, followed by incubation with antibodies targeting Nur77 or Ki67 in 1X Permeabilization buffer for 45 min at 4 °C (Invitrogen, 00-5523). All antibodies used in this study are listed in Extended Data Table 7. We excluded dead cells from the analysis by staining with Zombie Aqua, Green, Yellow and NIR Fixable Viability Stains (BioLegend, 423101, 423112, 423104, 423106) or 0.8 µM Alexa Fluor 750 NHS (Invitrogen, A20011). For the determination of absolute cell numbers, CD45high leukocytes and CD45med microglia were quantified using Precision Count Beads (BioLegend, 424902). Data were obtained using a BD Symphony A3 flow cytometer (BD Biosciences) and analyzed using FlowJo version 10.9 (BD Biosciences).

Instrument

For immune cell characterization by flow cytometry: BD Symphony A3 flow cytometer (BD Biosciences)
For flow cytometric nuclei/cell sorting: BD FACS Aria III Cell Sorter (BD Biosciences)

Software

For immune cell characterization by flow cytometry: FACSDiva software version 9.1 (BD Biosciences) and FlowJo version 10.9 (BD Biosciences).
For flow cytometric nuclei/cell sorting: BD FACSDiva v9.0.1 (BD Biosciences)

Cell population abundance

The frequencies of all analyzed cell/nuclei populations is depicted in the representative gating strategy.

Gating strategy

Gating strategies for all analyses are included in the Extended Data Figures.

☒ Tick this box to confirm that a figure exemplifying the gating strategy is provided in the Supplementary Information.